NGU Report 2006.081

A study of large-scale basins and comparison to the Eastern Barents Sea basins

NGU
Norges geologiske undersøkelse
Geological Survey of Norway

Geological Survey of Norway
NO-7491 Trondheim, Norway
Tel.: 47 73 90 40 11
Telefax 47 73 92 16 20

REPORT

Report no.: 2006.081 | ISSN 0800-3416 | Grading: Confidential to 31.12.2011

Title:
A study of large-scale basins and comparison to the Eastern Barents Sea basins

Authors:
Carla Braitenberg & Jörg Ebbing

Client:
Statoil ASA

County:

Commune:

Map-sheet name (M=1:250.000)

Number of pages: 71 Price (NOK):
Map enclosures:

Fieldwork carried out:

Date of report:
24.11.2006

Project no.:
3133.00

Person responsible:
Odleiv Olesen

Summary:

Detailed study of the gravity field and the isostatic state of the Barents Sea Region shows that the Eastern Barents Sea basins are not typical rift basins. They show distinctive features as large wavelengths, high lithospheric mantle density, thick sequence of sediments, a flat Moho and high elastic thickness, which are normally associated with cratonic or intracratonic basins. To understand the underlying cause of the Eastern Barents Sea basins, we make a comparison to well studied cratonic basins. For these basins, the structure, subsidence history and temperature evolution is relatively well known. We study the West Siberian basin, as an adjacent large-scale basin, the Michigan basin in North America, the Solimões, Amazon, Parnaìba and Paranà basins in South America, the Tarim basin in Central Asia and the Congo basin in Africa. The analysis includes the characterization in terms of gravity signal, geoid undulations, isostatic state, age and igneous activity.

An important point for the sediment evolution is the presence of the volcanism and the relative age of the volcanic strata with respect to the sedimentary package. In all the considered basins, except the Congo basin, volcanic masses are present at some stage and at some depth the basin.

All the basins show also deviation from the classic isostatic equilibrium model that predicts the crustal thickness (thinning in this case) from the topographic and sedimentary load. Instead of crustal thinning, high density masses in the crust and mantle appear to be a typical feature.

Keywords: Geophysics	Continental Shelf	Research
Gravimetry	Magnetometry	Isostasy
Report		

CONTENTS

1 INTRODUCTION

In recent years, the Barents Sea has recorded renewed interest as the other Arctic basins, and especially the large sedimentary basins are promising with regard to economical hydrocarbon potential. Detailed knowledge of the lithospheric structure, including the tectonic setting, the depth to basement and the crustal thickness are important input information to geodynamic modelling and study of the formation history of the basins.

Lack of well-log information in the Eastern Barents Sea means that the pre-Triassic geology of the basin is not well known. Shallow-marine carbonates were deposited throughout the Barents region during much of Late Palaeozoic times, but in Permian times, or possibly as early as Late Carboniferous times, these are replaced by marine sandstones and mudstones in the centre of the South Barents Sea basin (O'Leary et al. 2004). The Late Permian–Early Triassic period appears to have been a time of major basin formation, with subsidence accommodating the accumulation of more than 7 km of sediments in the basin centre. The predominantly Triassic succession is overlain by paralic and shallowmarine Lower–Middle Jurassic sandstones and mudstones and by Upper Jurassic deep marine mudstones. The Cretaceous period is represented principally by Neocomian shallow-marine clastics around the basin margins and by shales in the basin interior. Upper Cretaceous–Cenozoic rocks are thin or absent, owing in part to Cenozoic uplift and denudation.

For the Eastern Barents Sea basins the temporal data resolution is poor and therefore it is difficult to constrain the Palaeozoic history. None the less, O'Leary et al. (2004) observed increased subsidence rates, and hence strain rates, at similar times to the Timan–Pechora basin. Thus they interpret this as evidence for Ordovician-Silurian rifting events. It is not possible to say whether this event represents one or two separate events, as is sometimes the case for the Timan–Pechora basin. The Middle–Late Devonian rift event is better constrained. Most dramatic is the extremely rapid subsidence from latest Carboniferous to earliest Triassic times (300–240 Ma). This subsidence event is penecontemporaneous with the Permo-Triassic event seen onshore in Timan-Pechora, but yields much higher peak strain rates and thus higher stretching factors (β>3) than onshore (O'Leary et al. 2004). If this rapid subsidence event is related to rifting in the South Barents Sea, the Permo-Triassic succession represents an extremely thick syn-rift sequence.

O'Leary et al. (2004) argue that the Permo-Triassic rift event is the principal cause of subsidence, as the timing of this subsidence episode also coincides with a rift event identified on seismic data (e.g. Baturin *et al.* 1991; Johansen *et al.* 1992; Otto & Bailey, 1995). Thus the Permo-Triassic history of the whole region is one of coeval collisional and extensional tectonics. Foreland basin formation on the eastern margin of the Timan–Pechora basin was accompanied by significant extension offshore in the South Barents Sea basin and also, to a lesser extent, in the Timan–Pechora basin.

The North Barents Sea basin underwent a similar tectonic history as the South Barents Sea basin. Prior to the Late Permian, only a single basin existed in the region (Ostisty & Cheredeev, 1993). O'Leary et al. (2004) interpret that a Early to Middle Palaeozoic rifting was responsible for the formation of both basins and that the basins were separated following uplift of the Ludlov Saddle in Triassic times as a consequence of late stage Uralian shortening (Ostisty & Cheredeev, 1993). This uplift event was preceded by rapid subsidence associated with the Permian rift phase, which affected the whole Barents Sea basin.

Within the thick Upper Permian–Triassic terrigenous sediments (10–12 km) in the Northern Barents Sea significant quantities of magmatic bodies (intrusive and effusive rocks) are found, clearly connected to a main phase of rifting in Upper Permian–Triassic time (Ivanova et al. 2006).

Being a remote and very large area detailed geophysical data (e.g. seismic data), are only partly available. Therefore alternative approaches must be used in order to obtain a more complete picture of the tectonic framework. Detailed study of the gravity field and the crustal loading in the Barents Sea (Ebbing et al., 2005, 2006) has revealed that the region has very distinct features from an isostatic point of view. The Western and Eastern Barents Sea contain a series of deep sedimentary basins of more than 10 km thickness with very different characteristics, when considering the wavelengths involved: the Eastern Barents Sea Basins are very large (length 1400 km, width 550 km), whereas the Western Barents Sea basins are characterised by much smaller cross-wavelengths. This observation is an indication of a different formation history of the basins and may be correlating with different crustal properties.

Studies of the isostatic state of the lithosphere in combination with studies of the gravity field constrained by seismic data have shown that a clear transition exists between the Eastern and Western Barents Sea. This is expressed by the different features of the sediment thickness, but more important by changes in the lithospheric mantle density (Ebbing et al. 2005, 2006, in prep.). The relevant fields and main results are summarized in Figures 1.1-1.4. One of the most interesting results of the isostatic study was that the mantle densities, calculated by the isostatic and gravity inversion, show that the Eastern and Western Barents Seas are not one homogeneous province. As a result of the isostatic study, the Eastern Barents Sea basins have been interpreted as intracratonic basins. While this interpretation is speculative, there is no doubt about the large-wavelength inherited in the basin geometry.

The question arises, whether the features of the Eastern Barents Sea are similar to the properties of other large-scale, stable platform or intracratonic basins. Globally, a number of well-studied basins exist, which could be used in characterizing the Barents Sea basins. For this comparison, several consecutive steps are necessary: (1) a screening of existing large-scale basins has to be made, (2). the basins must be classified in terms of their properties. (3) Comparison to the Eastern Barents Sea basins to verify whether the dominant features discussed above are specific to the Eastern Barents Sea basins or common to large-scale basins. The analogies to other basins should allow setting some constraints on the possible evolution of the basins. The interest is not only focussed on the Eastern Barents Sea, but also on the neighbouring areas, the final investigations will include a detailed analysis of the properties of the upper lithosphere also for the Western Siberian Basin and its northward transition to the Kara Sea.

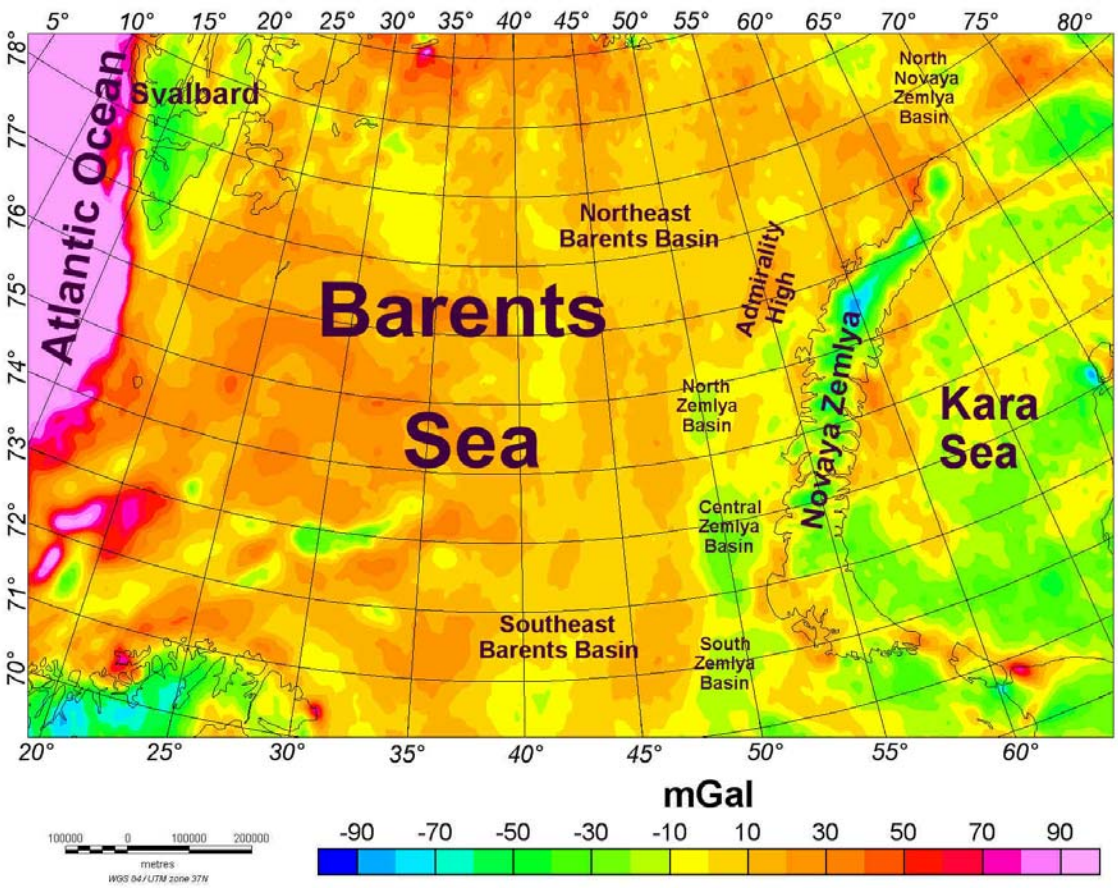

Figure 1.1. *Bouguer anomaly map of the Barents Sea Region. The complete Bouguer reduction was calculated with a reference density of 2670 kg/m^3 for onshore and offshore regions. The ice cover on Novaya Zemlya has been removed applying a density of 921 kg/m^3 (Ebbing et al. 2005)*

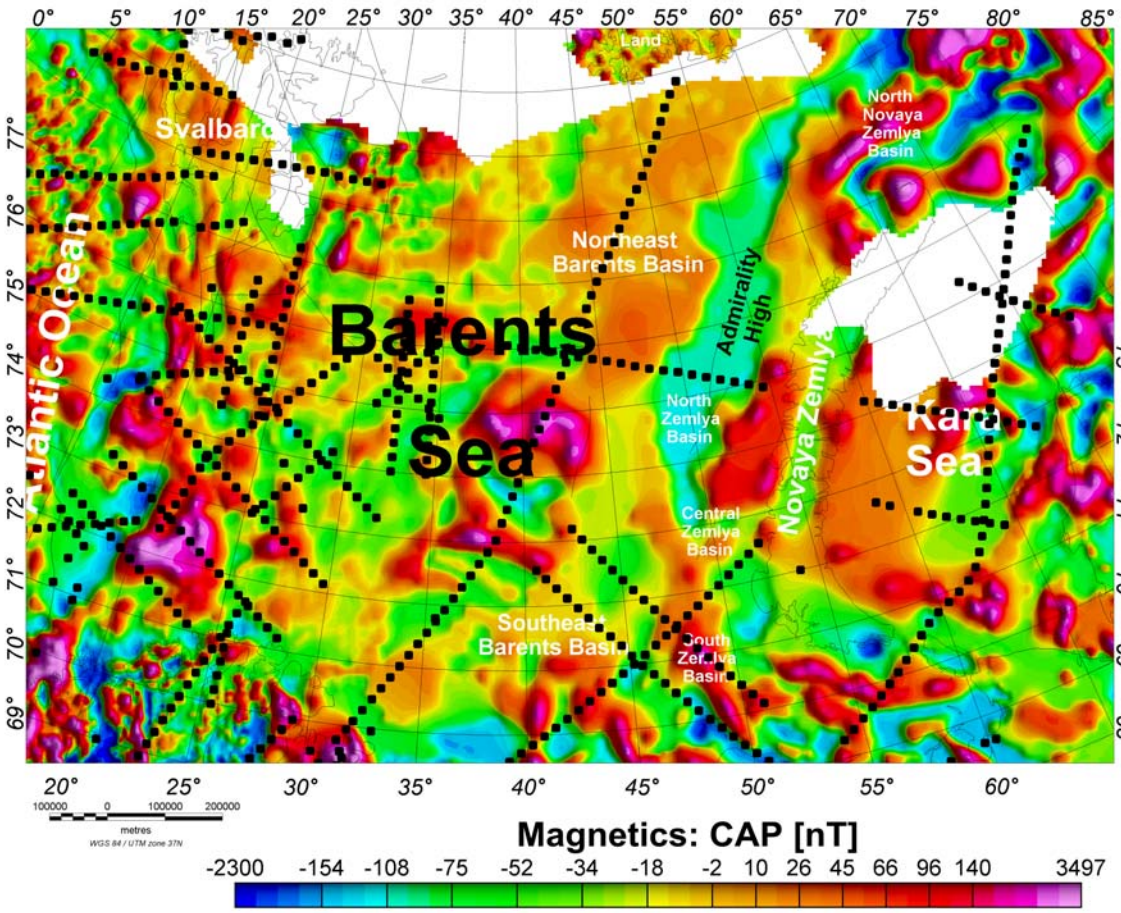

Figure 1.2 *Barents Sea Region: Magnetic anomaly map from the Gamma Project (after Verhoef et al. 1996)*

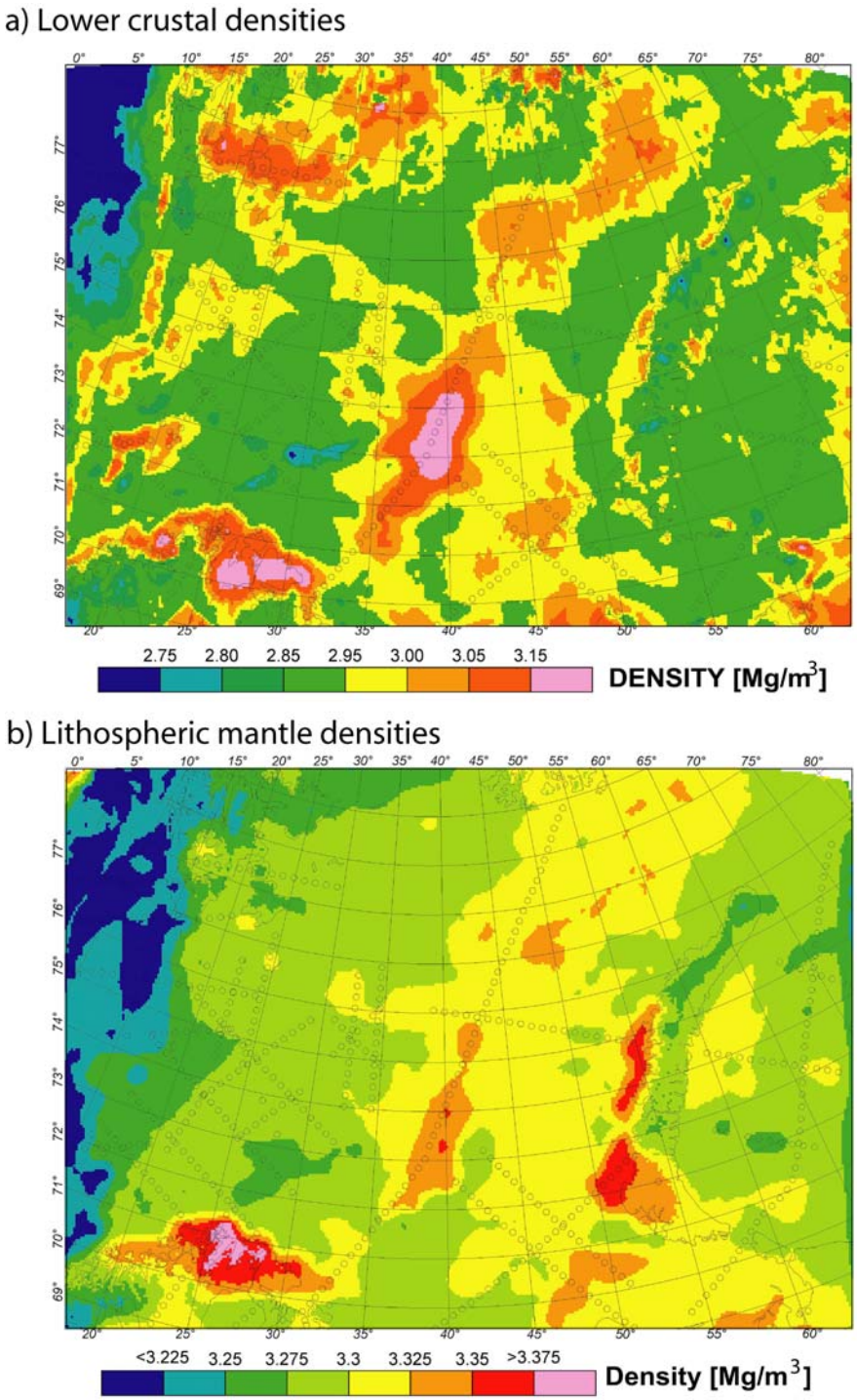

Figure 1.3 *(a) Computed lower crustal density variations and (b) Lithospheric mantle density to achieve local isostatic equilibrium and model the observed gravity field (Ebbing et al. 2006, in prep.).*

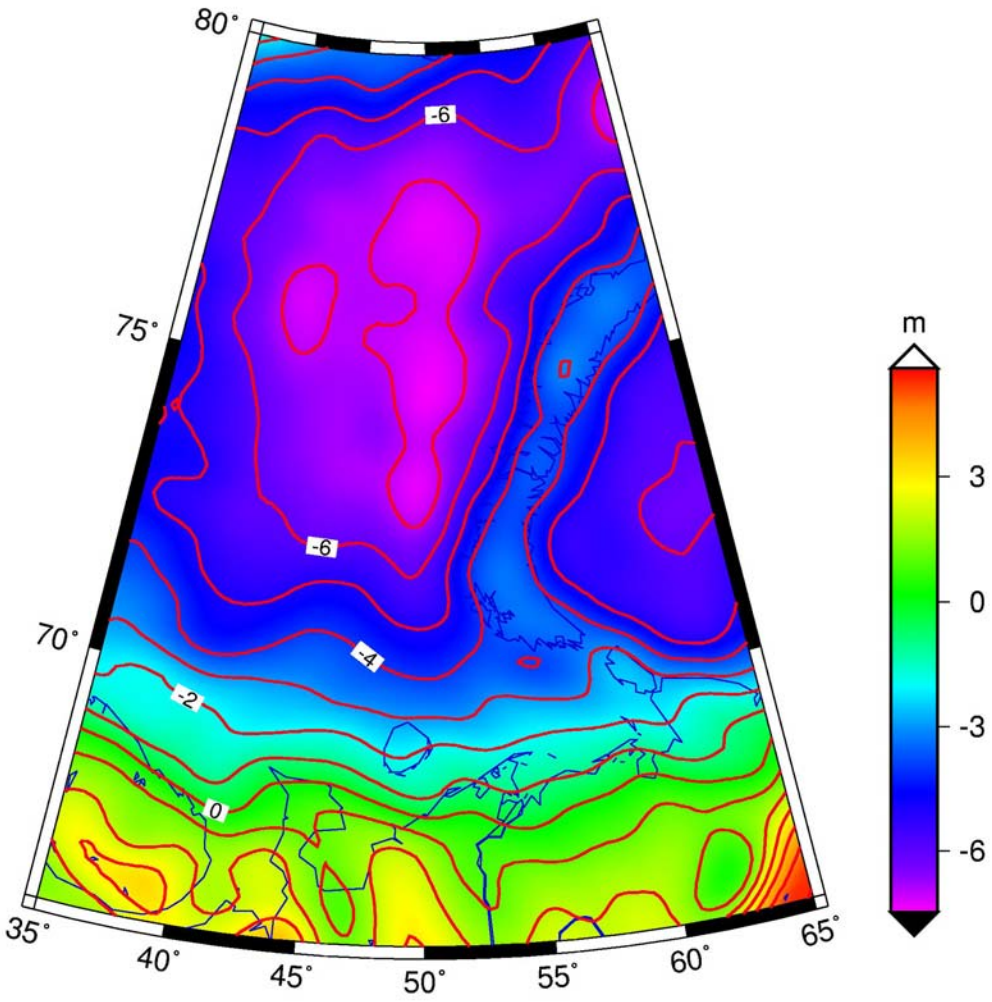

Figure 1.4 *Residual geoid for the East Barents Sea Region. The geoid undulations up to order and degree 360 have been highpass filtered by eliminating all variations with wavelength less than about 2000 km. This was accomplished by subtracting the geoid up to order and degree 10.*

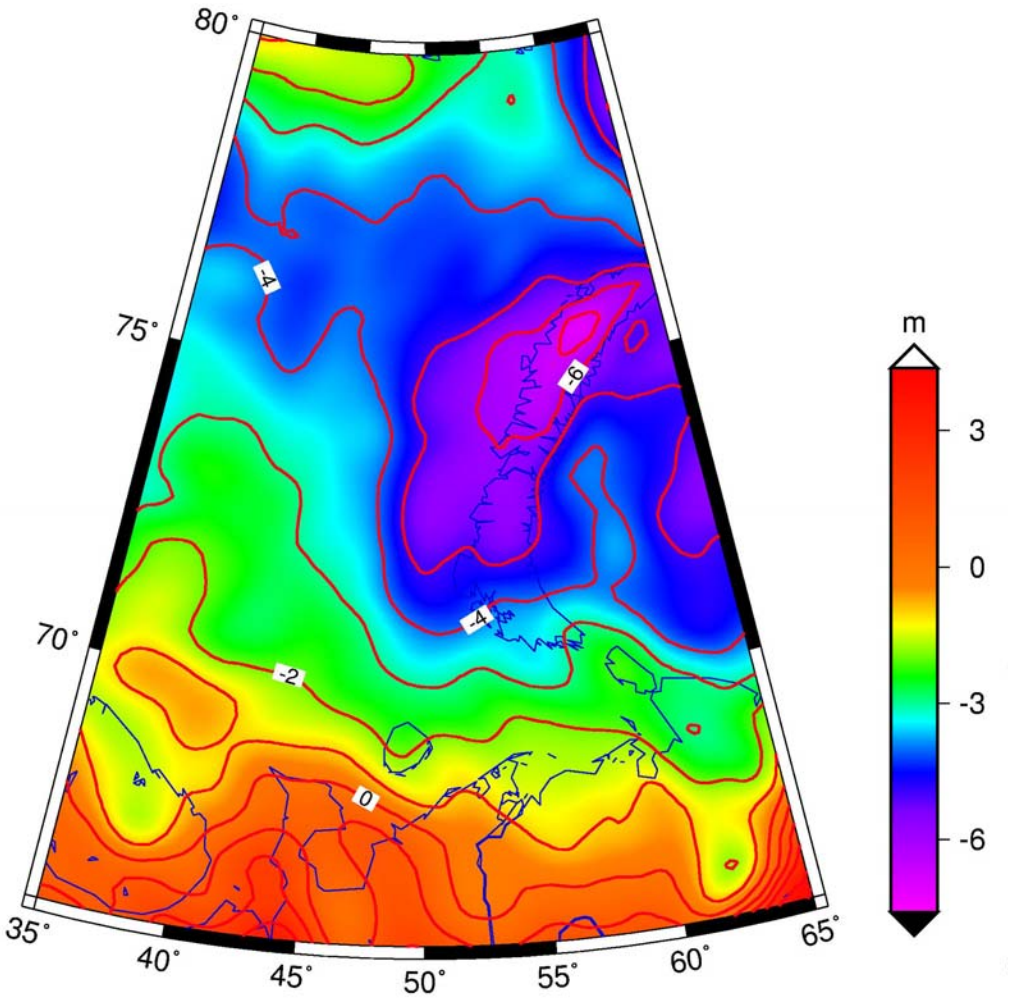

Figure 1.5 *Residual geoid terrain corrected – East Barents Sea Region. The residual geoid from Fig. 1.4 was terrain corrected. Reduction density: 2670 kg/m^3.*

2 INTRODUCTION TO LARGE-SCALE BASINS AND THEIR RELATION TO THE EASTERN BARENTS SEA

2.1 General features

A craton is generally defined as a part of the Earth's crust which is no longer affected by orogenic activity. In order to be defined a craton, stability has existed since 1000 Ma. In the following we consider both intracratonic and cratonic basins. The distinction between the terms is often not unambiguous and also not clearly defined in literature (e.g. Allen & Allen, 2005, Watts; 2001). We use the term intracratonic basins as a description of their position within a stable craton.

Intracratonic basins (Watts, 2001, p. 370; Leighton and , 1990) differ greatly from rift-type basins by several distinctive features, which can be summarized as follows:

- Episodic subsidence, continuous for hundreds of millions of years, can be piecewise linear
- Presence of inhomogeneities in lower crust or upper mantle
- Some basins are underlain by rifts
- Absence of uplift prior to subsidence
- Concentric nature of outcrop
- No crustal thinning

Examples which have the above properties in common are the well-studied Michigan and Illinois basins, the Williston basin, the Hudson Bay, the Congo basin and the Paris basin. The absence of crustal thinning is of particular interest, as it is one distinctive feature of the Eastern Barents Sea basins. If we consider the theory of isostatic equilibrium, the crustal loads must be compensated at a lithospheric level. In areas of young crust, crustal thickness is generally responding to the crustal loads: high topography is underlain by thick crust, while ocean basins have a thin crust, and large sedimentary basins are found do have a shallower crust. This simple relation is also the base of the McKenzie rifting type (McKenzie 1978).

Oceanic basins and sedimentary basins act as a negative load, as the average crustal rocks are replaced by lighter masses, e.g. the ocean water or the sediments. In the case of large sedimentary basins, which present a mass deficit, the absence of crustal thinning points to the

presence of compensating masses either in crust or upper mantle. The presence of the anomalous compensating masses are important in the context of the formation history of the basin, as they can be the cause of a downwarp of the crust due to the extra load, and the formation of the basin.

Another distinctive feature we find for the Eastern Barents Sea basins, but that does not apply to the Western Barents Sea basins, is the concentric nature of the basins. The Eastern Barents Sea basins are very wide and deep, in contrast to the Western Barents Sea basins, which are deep and relatively narrow, and are found in parallel groupings. This may be an indication, that the Eastern Barents Sea basins have a formation typical of cratonic basins, while the western basins are generated by extensive crustal forces (rifting).

The nature and mechanism of intracratonic basin formation is poorly understood, and various different mechanisms have been used to explain their subsidence. According to Sleep et al. (1980) cratonic basins have the following characteristics:

- Few to several hundred km width
- 3-20 km of flat-lying to gently dipping sediments. Thickening towards the centre
- Faulting can be present, but not dominant
- Subsidence lasts over periods of more than 100 10^6 years

Also considering these general properties, the Eastern Barents see basins have the required features, as e.g. large lateral extent, up to 20 km deep sediments, and a long subsidence history.

The models for the formation of cratonic basins have been summarized by Sleep et al. (1980), who propose different hypotheses for the formation:

1) Sediment loading:

The accumulation of sediments in an initially small depression leads to a positive feedback, until isostatic equilibrium is reached. A crude estimate of the total accumulation of sediments is described by the expression of Sleep et al. (1980):

Total accumulation of sediments:

$$d' = \frac{\rho_m - \rho_w}{\rho_m - \rho_s} d \qquad \text{(Eq. 1)}$$

where d = initial depression, d' = sediment accumulation, and ρ_m, ρ_s, ρ_w are the densities of mantle, sediments and water respectively. By inserting typical values into Equation (1) the total accumulation is estimated to be about a factor three greater than the initial depression.

2) Thermal cooling

By thermal cooling the depth to a certain layer increases with time according to the relation:

$$d = U_0(1 - e^{-age/t_0}) \qquad \text{(Eq. 2)}$$

where d=depth to bed, U_0 depends on position, and t_0 is the thermal time-constant.

3) Phase changes-metamorphism

If the subsidence is due to a loading at the base of the crust, it could be due to a densification of the lower crust concomitant with a heating event. A possible scenario could be intrusion of basaltic material during heating event, which is subsequently transformed to eclogite, similar to processes observed at volcanic margins.

Another hypothesis is that the lower lithosphere below the Moho is affected by a densification which constitutes a surplus load. The load will be acting as a down-warping force to the crust, in the case that the lower lithosphere is mechanically consolidated to the crust. In the case of the lower lithosphere being weakly connected to the crust, a high-density lower lithosphere will create a more buoyant lower crust and thus cannot act as a down-warping force.

Within the frame of the isostatic modelling of the Congo basin Hartley and Allen (1994) and Hartley et al. (1996) made a summary of hypotheses for the formation of large-scale basins. In addition, and partly in superposition to the above, the most relevant are:

- Lithospheric stretching and thermal contraction
    - Rifting associated with thermal plume
    - Thermal contraction following heating
- Crustal and mantle phase changes, metamorphism and intrusion
    - Phase changes and thermal metamorphism
    - Isostatically uncompensated excess mass due to igneous intrusions
- Changes of in-plane stress and tectonic rejuvenation
- Convective instabilities
- Subaerial erosion followed by sediment loading

2.2 Gravity and geoid fields of the basins

The Bouguer anomaly is mainly representing crustal sources and constitutes a blueprint for crustal thickness variations in younger tectonic areas. In the case of cratonic areas the base of the crust shows little variations, and the Bouguer anomaly is mainly featuring the density variations in the crust or upper mantle. The isostatic gravity anomaly, here equivalent to the Airy isostatic anomaly, can be used to identify additional loads. A positive isostatic gravity anomaly indicates under-compensation, a negative isostatic anomaly corresponds to over-compensation, and an isostatic anomaly of zero indicates isostatic equilibrium

Due to the different distance dependency of the gravity potential, the geoid undulations average the anomalies over a greater area and are representative generally of deeper lying structures with respect to the gravity field. We consider the geoid undulations reduced from the longest wavelength variations. We have systematically subtracted the geoid field up to degree and order 10 in the spherical harmonic expansion in order to obtain a field representative of crust and upper mantle structures. This reduction corresponds to subtracting the components of the field with wavelength greater than 2000 km at mid-latitudes. The terrain corrected geoid is the analogue to the Bouguer gravity field, and has been reduced from the effect of topographic masses.

For sedimentary basins the gravity field can be analysed to obtain information on the basin formation history. Nunn and Aires (1984) developed a rule of thumb for intracratonic basins: the large sedimentary basin is the source of a negative gravity signal, spatially covering the entire basin. A high-density body in the crust, which contributes to the subsidence of the basin (during formation), produces a localized gravity high over part of the basin. It will be flanked by negative anomalies, originating from the low-density sediments. If the high-density body is situated in the upper mantle, the gravity high is weaker and has a longer wavelength, so that the complete gravity signal will be near zero or negative.

Large-scale basins characterised by a central gravity high are the Illinois, Williston, and the Amazon basins. However, a central gravity high is not found in all intracratonic basins. The Central Australia, Parana', Congo, Paris and Hudson bay basins have a gravity low associated with the basin. The gravity lows contradict models in which dense rocks have intruded into the crust, since this would produce a gravity high. Thinning of the crust can also be ruled out,

as this would have the same gravity effect as high density material intruded into the lower crust. Therefore, either the Moho in the Central Australia, Parana', Hudson bay, Congo and Paris basins is flat-lying, or it is deflected downwards (Watts, 2001). From our studies we may attribute the Eastern Barents Sea basins to the second type.

3 SCREENING CRITERIA FOR THE LARGE-SCALE BASINS

As mentioned above, our goal is to classify the deep East Barents Sea basins in the context of world-wide large-scale basins. We therefore must set up a list of screening criteria. Our screening criteria are the following.

- geometry of the basins, including area and lateral extent
- maximum extent of sediment thickness

  Together with the sedimentation history this datum is important to determine the time extent of basin formation, which has been found to be a distinctive feature. Large-scale basins tend to have accumulated sediments during time intervals in the order of at least 100 Ma.
- presence of magmatism

  this is tightly connected to the loading, contributing generally to high-density material acting as a positive load in the crust. Uncertainties exist about the exact amount of magmatism: E.g. in the Eastern Barents Sea magmatic material has been observed on seismics (Ivanova et al. 2006), but the exact amount cannot be estimated from single seismic profiles and therefore not be used in isostatic calculations.
- gravity and geoid

  The geophysical fields closest related to the crustal densities is the gravity field and the geoid. The geoid undulations signal density variations at greater depth with respect to the gravity anomalies. We consider the geoid undulations and the free air gravity anomaly, as well as their topographically corrected counterparts, the Bouguer gravity and the terrain corrected geoid undulations. The isostatic gravity anomaly is calculated, taking into account superficial as well as intracrustal loads, and the Airy-type isostatic compensation and the flexural type compensation.
- Seismic velocity models

  Seismic velocity models can be compared, where available, to the density structure derived from the inversion of the gravity field.

4 THE STUDIED BASINS

Our selection of basins is biased by the availability of relevant publications. The Michigan and Illinois basins are well studied and have been described as prototype cratonic basins (Watts, 2001) and were therefore included in the study. The Parana' basin has been set into relation to the West Siberian basin in terms of the magmatism, and was therefore added to the list (Reichow et al., 2005). The Amazon, Solimões and Parnaiba basins complete the picture of the Brasilian large-scale basins. The Tarim basin was chosen as being another example of a large dimension basin with great sedimentary thickness. And the West Siberian basin is of particular interest in our study since it borders the greater Barents Sea region. In the following table the geographic coordinates of the windows pertaining to the different basins are given.

Name of Basin, Cratons involved	Lat, min	Lat, max	Long, min	Long, max
Siberian traps	50	72	90	110
West Siberian Basin	50	72	58	90
Tarim Basin	35	45	74	90
Michigan Basin	42	48	-92	-80
Illinois Basin	37	44	-93	-86
Parana' Basin	-15	-25	-45	-56
Parnaiba Basin	0	-15	-30	-55
Amazon- Solimões basin	2	-10	-40	-75
Congo basin	-7	5	12	30

Table 4.1 *The considered basins and their geographic windows*

A summary of the ages of the sedimentary sequence, of the aerial extensions and of the thickness is given in Table 4.2. Further details can be found in Chapter 8. The basins have an aerial extension of at least 0.4 10^6 km^2 and a sedimentary history of at least 250 Ma. The thickness of the sediment columns varies greatly from a minimum of 4 km to a maximum of 20 km. All except the Congo basin have a certified presence of volcanic rocks, either as large aerial layer or in the form of volcanic intrusions.

East Barents Basins	Ordovician to Cenozoic Upper Permian-Triassic magmatic bodies	A=0.4 10^6 km^2 D < 20 km	Gramberg et al. (1999)Gramberg et al. (1999)
West Siberian Basin	Triassic to Cenozoic sediments. Permian–Triassic basalts (250Ma) overlying possible Permian continental deposits.	A=3.2 10^6 km^2 D < 8 km	Vyssotski et al. (2006)Vyssotski et al., 2006
Michigan	Cambrian Middle Ordovician to Jurassic. Middle Keweenawan (1100 Ma) volcanic sequence	A=0.5 3 10^6 km^2 D < 3 4 km	Nunn (1994) Sleep and Sloss (1978)
Amazon Basin and Solimoes Basin	Ordovician to Cenozoic. Late Triassic-early Jurassic magmatic intrusions (170-230Ma)	A=1.1 10^6 km^2 D < 5km	Milani and Thomaz Filho (2000)
Parana' Basin	Silurian-Cretaceous Flood basalts (137 to 130 Ma)	A=1.2 10^6 km^2 D < 7 km	Milani and Thomaz Filho (2000) An and Assumpção (2006)
Parnaiba Prov.	Silurian-Cretaceous. Two magmatic intrusions: Triassic-Jurassic (Penatecuaua magmatism) and early Cretaceous.	A=0. 61 10^6 km^2 D < 3.5 km	Milani and Thomaz Filho (2000) Almeida et al (2000)
Tarim Basin (area based on sediment thickness model) with Qaidam B.)	Cambrian-PaleoceneProterozoic-Quaternary Permian basalt layer.	A=1.10.8 10^6 km^2 D < 15 km	Chen and Shin (2003) Lithospheric Dynamic Atlas of China (1989)
Congo Basin	Late Proterozoic to recent	A=1.8 10^6 km^2 D < 9 km	Daly et al. (1992)

Table 4.2 *Ages, areal extension and thickness of the large-scale sediment basins considered in this study.*

5 PUBLIC DATABASES USED IN THE STUDY- PRESENT STAGE AND UPCOMING DATA

At the present stage of the work the analysis had to rely on public available data, as more specific local data have not yet been available. Gravity field data are available at a spatial resolution of 0.5°x0.5° using the recent GRACE satellite data integrated with terrestrial gravity measurements. We have adopted the solution of the GFZ Potsdam with coefficients of the spherical harmonic expansion up to degree and order 360 (EIGEN-GL04C, Förste et al., 2006). This solution is to be preferred to the solution GGM02 from NASA, due to the fact that the coefficients greater than n=120 for the GGM02 solution have been taken from the EGM96 model, whereas the same coefficients of the EIGEN-GL04C solution have been recalculated. We use this expansion for obtaining the gravity field as well as the geoid. By beginning of the year 2007 a new gravity field shall be released, with spherical harmonic coefficients up to degree and order 1240, allowing a 3–fold resolution in space. The applied digital elevation model (DEM) consists of the 1-km grid GLOBE (Global Land One-km Base Elevation) released by the National Geophysical Data Center in Boulder, CO (NGDC). The DEM is indispensable for calculating the isostatic loading and for correcting the gravity data for the effect of topography.

Topographic correction of gravity and geoid fields

The combined satellite and terrestrial gravity fields must be corrected for the topography in order to obtain the Bouguer anomaly and the geoid counterpart of the Bouguer anomaly. It is useful to correct the data for the topography, as then the crustal masses are more evident in the maps. We use the DEM mentioned above for the near field reduction, and have computed a coarse grid (0.1° resolution) from the above DEM for the far field reduction. The computation is based on two digital elevation models, a detailed and a coarse one, which is used in the inner (<10 km) and outer zones (10 to 167 km), respectively. Calculations are computed for a spherical Earth, by using the approximation with prisms, following the procedure proposed by Forsberg (1984).

We have considered the use of the publicly available Moho depth model and sediment thickness model of the global crust 2.0 (Bassin et al., 2000; CRUST 2.0, 2006). The Moho is available at the resolution of 2°x2°, which is too low for our purposes. The sediments are available at the resolution of 1°x1°, which also is a rather crude estimate for our study. For the

Tarim basin we have a Chinese sediment-thickness grid at hand (Lithospheric Dynamic Atlas of China, 1989). For the West Siberian Basin a basement depth model was provided by Statoil.

6 WEST SIBERIAN BASIN

6.1 Ages and geometry

The West Siberian Basin (Fig. 6.1) (WSB) is one of the largest intracratonic basins of the world, with an areal extent of approximately $3.2x10^6$ km^2 (corresponding to the basin outline reported in Fig. 6.1a). Published values vary according to the adjoyning basins that have been included (e.g. Vyssotsky et al., 2006). Figure 6.2 shows the basement depth for the West Siberian basin. The deepest part of the basin is found in the northern half, connecting to the Yenisey-Khatanga deposits continuously, without the presence of a dividing high. In the southern half the basin widens, but the deepest part (thickness > 5000m) is elongated and relatively narrow, indicating smaller characteristic wavelengths. In the southern part of the basin we find a succession of NNW-SSE linear-oriented lows in the basement. The basement of the WSB consists of Baikalian (Late Precambrian), Caledonian (Cambrian-Silurian) and Variscan (Silurian-Permian) fold systems. A graben system limits the northern part of the basin (Pur-Taz region and Kara Sea). Late Permian evolution is associated with the Siberian flood basalts and intrusives and the basalts appear to cover the entire basin (Vyssotski et al., 2006). The age of the flood basalts is about 250 Ma, with an extrusion time of less than 1 Ma. The volcanic eruption was followed by basin-wide subsidence, bringing the basalts down to a depth of 6400 m. It is interesting to note that the flood basalts on the East Siberian platform remained superficial, pointing to a different buoyancy between the WSB and the East Siberian platform. The post-volcanic stratigraphic section has been analysed by Vyssotski et al. (2006) and covers the Mesozoic to Cenozoic. A Moho map is reported in Vyssotski et al. (2006) based on an older work of Kovylin (1985). The crustal thickness varies between 36 and 42 km, and the central part has a thickness of 40 km, flanked by lower values (38 km). Towards the Siberian platform and the Urals the Moho deepens to a value of 50 km. To the north the crustal thickness thins to a value of 34 km in the Kara Sea. The Moho depths in E-W direction are generally shallower beneath the basin compared to the Urals and to the Siberian platform. In NS direction the depths vary from 34 km to 42 km along the central part of the basin. The Moho depths do not show any depth variation correlated to the Yenisey-Khatanga deposits, although these are over 10000 m thick.

6.2 Gravity and geoid - West Siberian Basin

The gravity anomaly over the central area of the WSB is between -5 and -25 mGal (Fig. 6.4). Three linear highs emerge clearly in the northern part of the basin, and are probably associated with structures in the Paleozoic basement, as can be seen by comparing the profiles 27, 31 and 19 of Vyssotski et al. (2006). These structures are though not evident in the gridded basement depth map (Fig. 6.2). This may be due to an interpolation smoothing effect of the gridded values. The basin is bounded by positive gravity anomalies: the Urals (+ 60 mGal), the Kazakh highlands to the South (20 mGal) and the East Siberian platform to the east. The Bouguer field (Fig. 6.5) has very similar features to the gravity anomaly in the WSB: the basin has generally negative anomalies, oscillating around -15 mGal. The Urals and the three positive linear features noticed in the gravity anomalies remain. There is though a general decrease of the anomalies towards SE, leading to the Kazkh high-planes and the Altai ranges (Compare to topography map, Fig. 6.1b). The decrease is surely due to crustal thickening in isostatic response to the increase in topography. The Urals do not show the decrease in Bouguer gravity, which is evidence that the crustal thickness does not respond isostatically to the Ural range. The terrain corrected geoid is interesting, as it repeats the low northern positive linear features, observed in the gravity field, indicating that these are major features affecting not only the basement, but probably also the lower crust. Only detailed modelling can though give more quantitative and definitive results. Considering the geoid residual (Fig. 6.6), the basin lies in a concentric geoid low. The central part of the basin has a general decrease in the geoid height with higher values surrounding the basin, e.g. the Urals show a broad geoid high. The terrain corrected geoid (Fig. 6.7) is interesting, as it repeats the northern positive linear features, observed in the gravity field, indicating that these are major features affecting not only the basement, but probably also the lower crust. The deepest part of the basin lies in a geoid minimum (A in Fig. 6.7). The two relative geoid highs (B & C in Figure 6.7) correspond to the two areas with shallower basement. Only detailed modelling can though give more quantitative and definitive results.

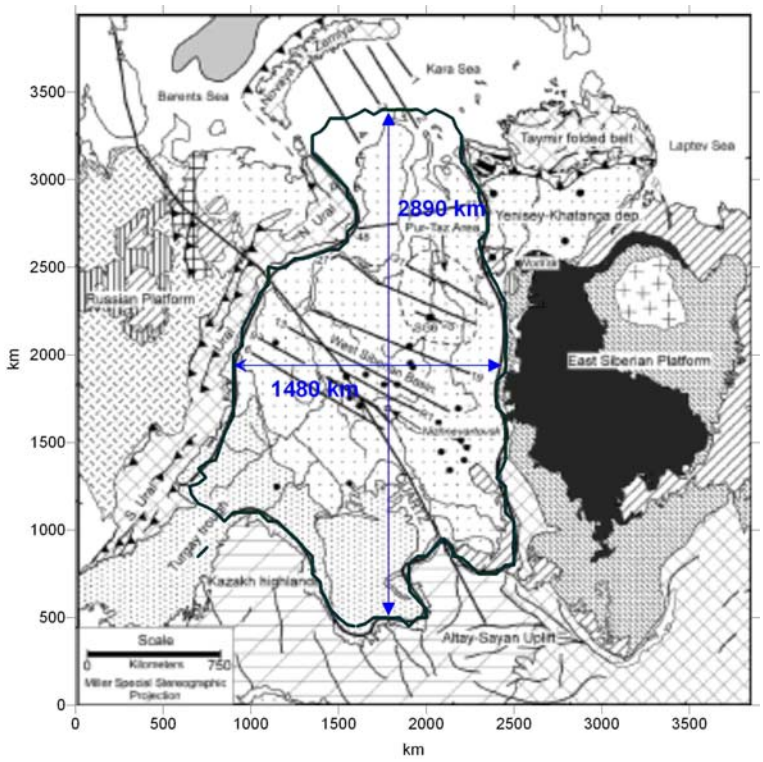

Figure 6.1a West *Siberian Basin: basin geometry. (Vyssotski et al., 2006). The basin is outlined in dark green. The northward extent of the basin is at present not defined. Blue arrows indicate the length and width of the basin.*

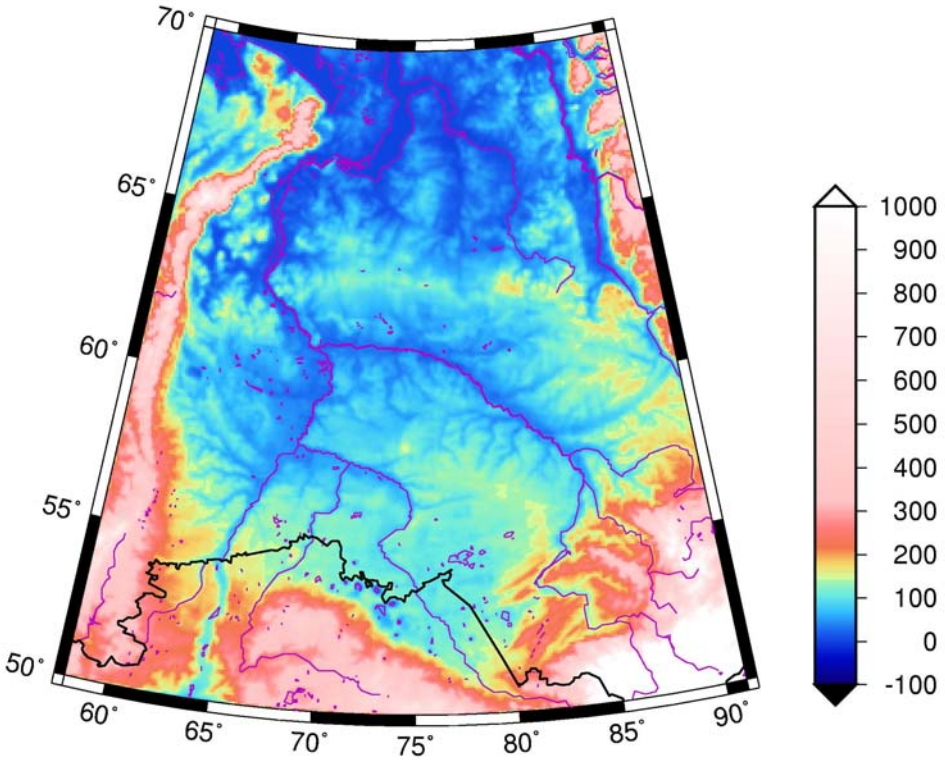

Figure 6.1b *Topography (m) of the West Siberian basin area. National borders (black) and coastline and rivers (blue).*

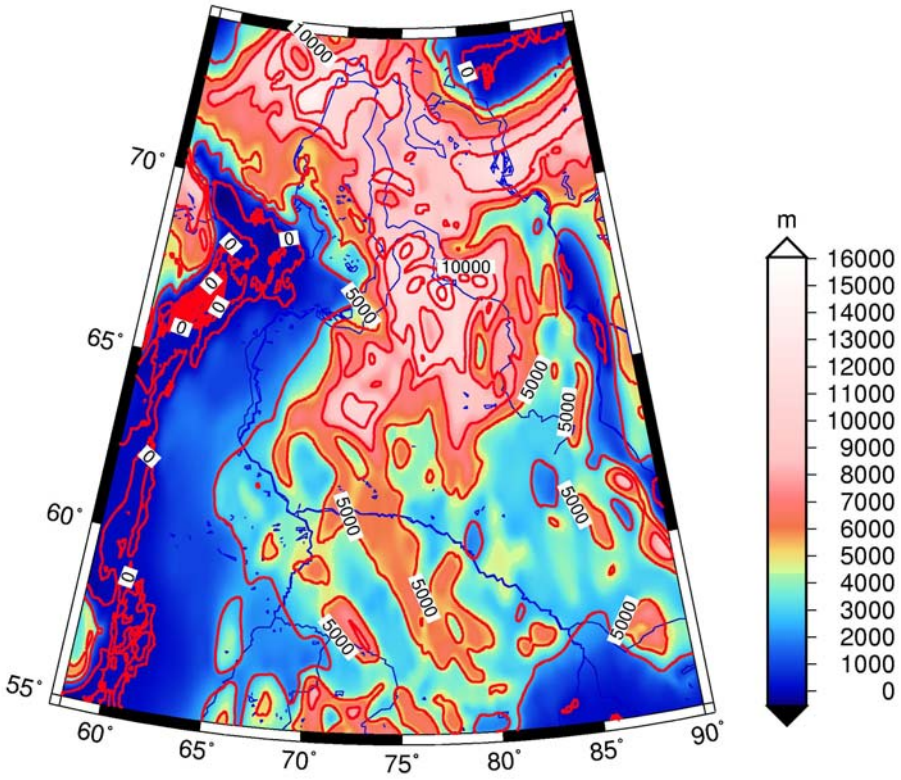

Figure 6.2 *Gridded basement map (m). Statoil database.*

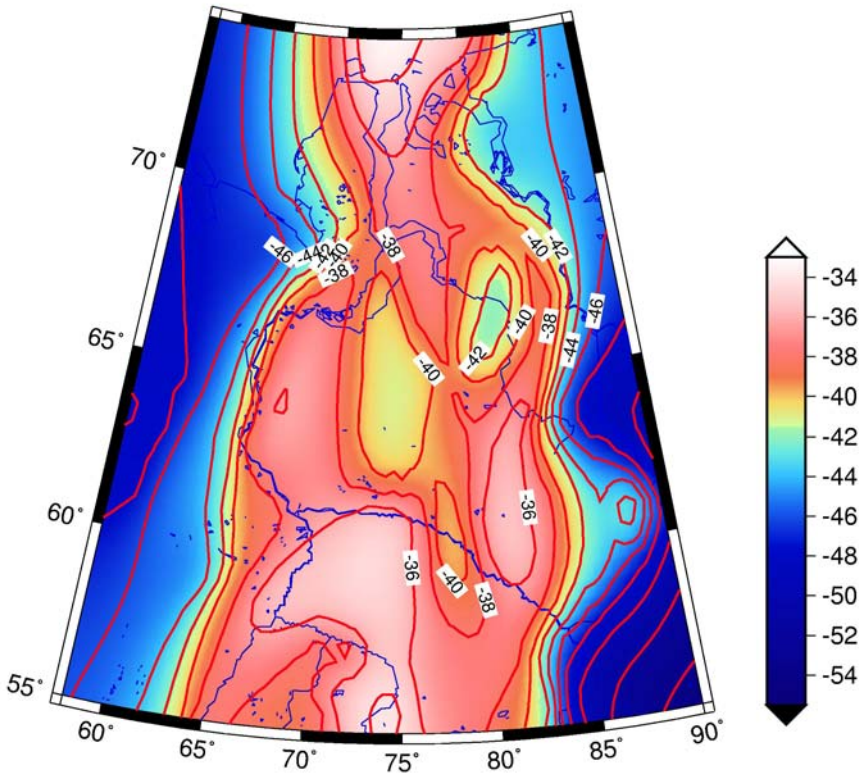

Figure 6.3 *Moho depth map (km) for the West Siberian basin area. Digitised from Vyssotski et al. (2006) based on an older work of Kovylin (1985).*

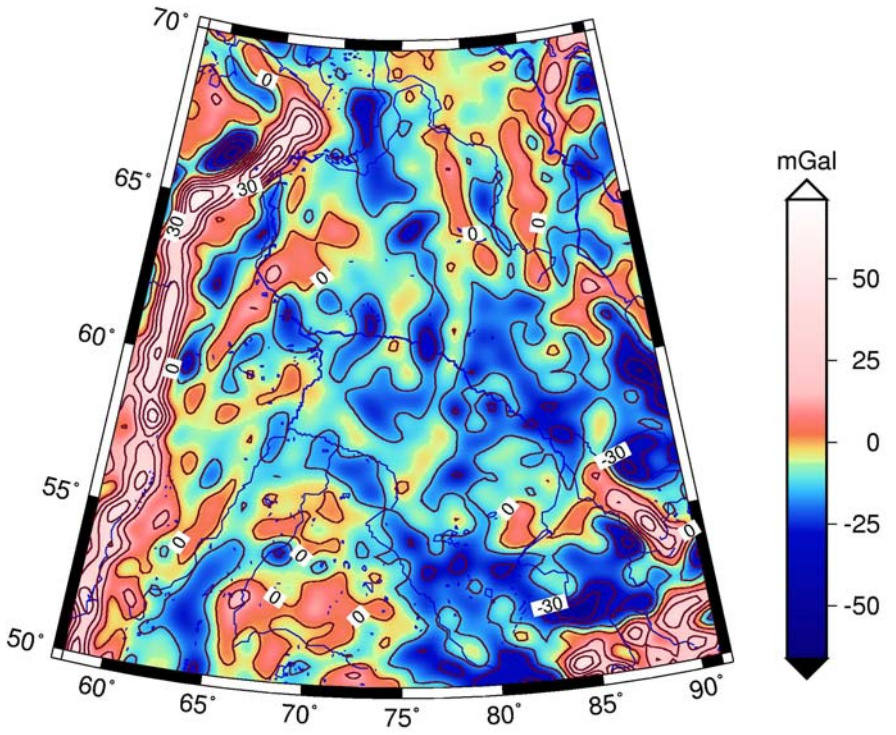

Figure 6.4 *Gravity anomaly (mGal) for the West Siberian basin area. (Data: EIGEN-GL04C, Förste et al., 2006). Coastline and major rivers in blue.*

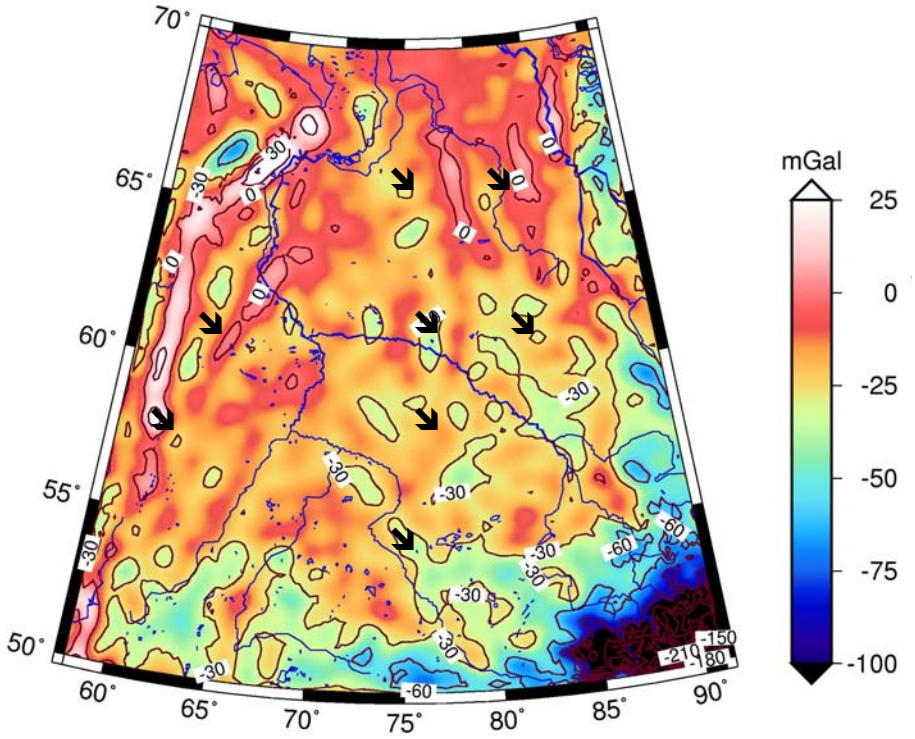

Figure 6.5 *Bouguer gravity anomaly (mGal) for the West Siberian basin area. (Data: EIGEN-GL04C, Förste et al., 2006). The linear gravity highs are marked by black arrows.*

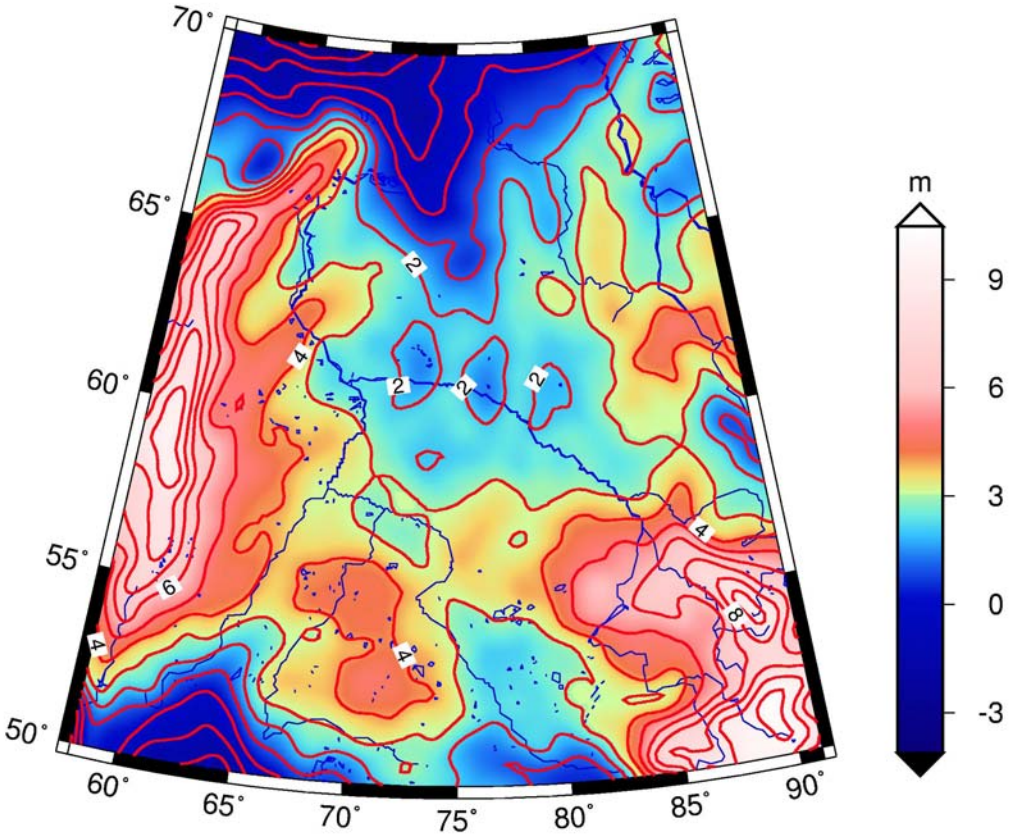

Figure 6.6 *Geoid residual (m) for the West Siberian basin area. Data: EIGEN-GL04C (Förste et al., 2006) freed from lowest degree and order (up to degree and order 10) harmonic components.*

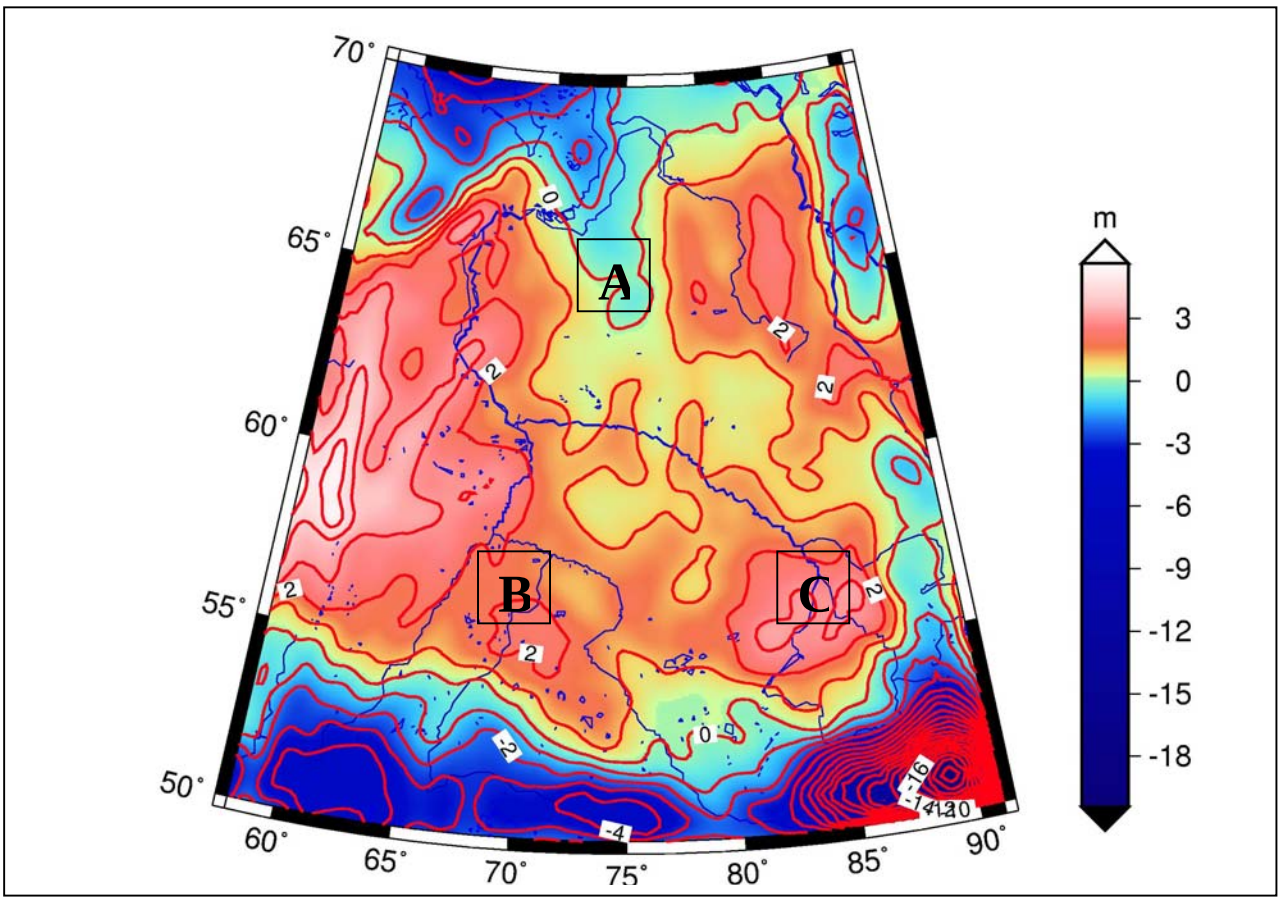

Figure 6.7 *Geoid residual terrain corrected (m) for the West Siberian basin area. Data: EIGEN-GL04C (Förste et al., 2006) freed from lowest degree and order (up to degree and order 10) harmonic components. A: geoid low correlated to deepest part of the basin. B, C: geoid highs correlated to a shallowing of the basement.*

7 STUDY OF THE LARGE-SCALE BASINS

7.1 The Michigan basin

The Michigan is an intra-cratonic basin (location see Figs. 7.1.1a and 7.1.1b) that has been extensively analysed and modelled, and which therefore cannot be missed in a list of intracratonic basins. The ages of the sediments range from Middle Ordovician (462Ma) to Jurassic (136 Ma) (Nunn, 1994). The basin itself has a circular geometry with a diameter of about 700 km and a depth of up to 4 km (Fig. 7.1.2a,b). The basin width decreases with time, and an onlap of younger sediments at the edges of the basin is absent. Sleep and Snell (1976) attribute the decrease in width during the Mid-Ordovician to Pennsylvanian to the fact that the lithosphere can be modelled by a visco-elastic model with a Maxwell relaxation time of 1 Ma and a viscosity in a range of $4x10^{23}$ to $4x10^{24}$ Pa s. Controversially, Sloss and Scherer (1975) argue that the Michigan basin only appears to be decreasing with time, due to the effects of a basin-wide erosional event that has eliminated parts of the sedimentary deposits. Haxby et al. (1976) explain the subsidence history of the basin by an elastic flexure model, in which the elastic thickness (Te) decreases with time from a Te=30 km to a Te=60 km. The increase in elastic thickness is attributed to an initial high heat flow, leading to a relatively low Te. The high heat flow was attributed by the authors to a diapiric intrusion of hot asthenospheric material that metamorphosed the gabbroic lower crust to eclogite. The subsidence was in this view caused by a resulting increase in the lower crustal density. Also according to Nunn and Sleep (1984) the basin subsidence is governed by flexural deformation. The initial load is caused by thermal cooling, creating an initial depression. The sedimentary fillling of the depression gives an extra load, which leads to further subsidence, until isostatic equilibrium is reached. The thermal load is estimated to amount to about 20% of the sediment load. The authors declare that at the time of writing no volcanic masses in the basin had been found, which could be related to the heating event.

The presence of a NW-SE trending rift was shown by Zhu and Brown (1986). The red beds of the upper Keweenawan clastic assemblage and medium and coarse-grained mafic igneous rocks were found during a 5.4 km deep drilling near the centre of the basin (Zhu and Brown, 1986). The volcanic sequence rocks are up to 8 km thick in an up to 70 km wide rift basin. In a more recent paper Nunn (1994) considers free thermal convection beneath the basin as a driving force to explain the subsidence of the basin. The model explains the variable

subsidence rates, which alternate episodically between high and low values, and deviate from the exponentials associated with thermal contraction by conductive heat loss. Free thermal convection is defined as flow driven by spatial variations in fluid density caused by variations in fluid temperature. During periods of free convection heat loss is accelerated, causing a short burst of rapid subsidence. After free convection slows or stops, heat loss is depressed and the basin undergoes a longer period of slow subsidence until heat conduction from below again increases the temperature gradient in the upper crust. The vigour of free thermal convection depends on permeability and temperature gradient. In the subsidence model for the Michigan basin, the permeability is made to change due to closing and opening of fractures in the igneous body underlying the sediments. The tectonic subsidence is driven by the load imposed on the lithosphere due to the net loss in temperature, which leads to horizontal contraction of the crust.

7.1.1 Gravity and geoid in the Michigan basin

The Michigan basin is associated with a central gravity anomaly high flanked by lows. The gravity high is persistent in the gravity anomaly and in the Bouguer anomaly. We have collected for this area the terrestrial gravity data made available by BGI (Fig. 7.1.3), and the gravity anomaly from the joint analysis of GRACE satellite and terrestrial observations. Having a good terrestrial data set at hand, allows us to evaluate the GRACE-terrestrial gravity field compilation. The comparison of the two gravity-anomaly (Fig. 7.1.3a and Fig. 7.1.3b) compilations demonstrates that the GRACE-terrestrial data can be used for our purpose of comparison of cratonic basins. All main features are contained in the GRACE -terrestrial data. Also the geoid is available in the GRACE -terrestrial solution. The geoid residual (Fig. 7.1.5) is dominated by long-wavelength features and does not show evident correlations with the position of the Michigan or Illinois basins. This is very different with respect to e.g. the Tarim basin or the WSB basin. This could be due to the fact that the Michigan and Illinois basins are of much reduced areal dimensions compared to the other mentioned basins. It would also be an indication of the fact that existing density anomalies at depth below the Michigan and Illinois basin are not correlating with the shape of the two basins.

Zhu and Brown (1986) modelled the gravity field along the COCORP seismic section, which extends from the centre of the Michigan basin southwards. They find the basin being made up of 3.7 km nearly undeformed Paleozoic strata and the underlying Cambro-Ordovician

sequence. Below they suppose 4 km of clastic assemblage (Upper Keweenawan), which overlies about 8 km of the Middle Keweenawan volcanic sequence filling an about 70 km wide rift basin. The study implies that the rift basin was subsiding as it was filled by episodic volcanic flows and interflow clastics. In their 2D gravity model the gravity high is explained by the volcanic sequences, which have been modelled with a density of $2.95x10^3$ kg/m^3, surrounded by a $2.65\text{-}2.77x10^3$ kg/m^3 dense mid-crust.

7.1.2 Comparison to West Siberian and Eastern Barents Sea basins

The Michigan basin is comparable in size to the Eastern Barents Sea basin, but its depth reaches only 20% of that of the Barents Sea. With the Barents Sea and the West Siberian basin is shares the probable presence of an extinct rift that is invoked for the formation of the basin. The geoid signals differ in one important aspect, in that the Michigan and Illinois basins are not associated with a geoid low, whereas both the Barents Sea basin and the West Siberian basin are. This implies a different lithospheric structure below the basins, with greater wavelength features found in case of the Michigan and Illinois basins.

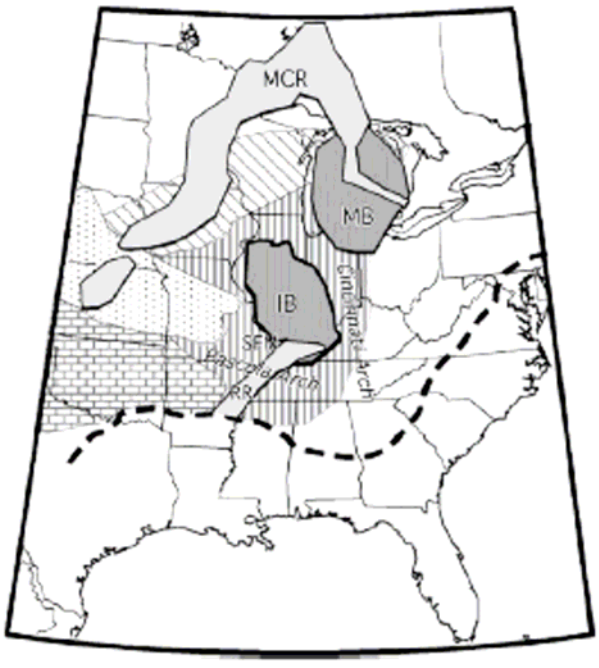

Figure 7.1.1a *Major tectonic provinces and Precambrian basement of the mid-continental United States. MCR- Mid-Continent Rift MB:- Michigan Basin, IB – Illinois Basin, RR - Reelfoot Rift and Rough Creek Graben (Bedle and van der Lee, 2006)*

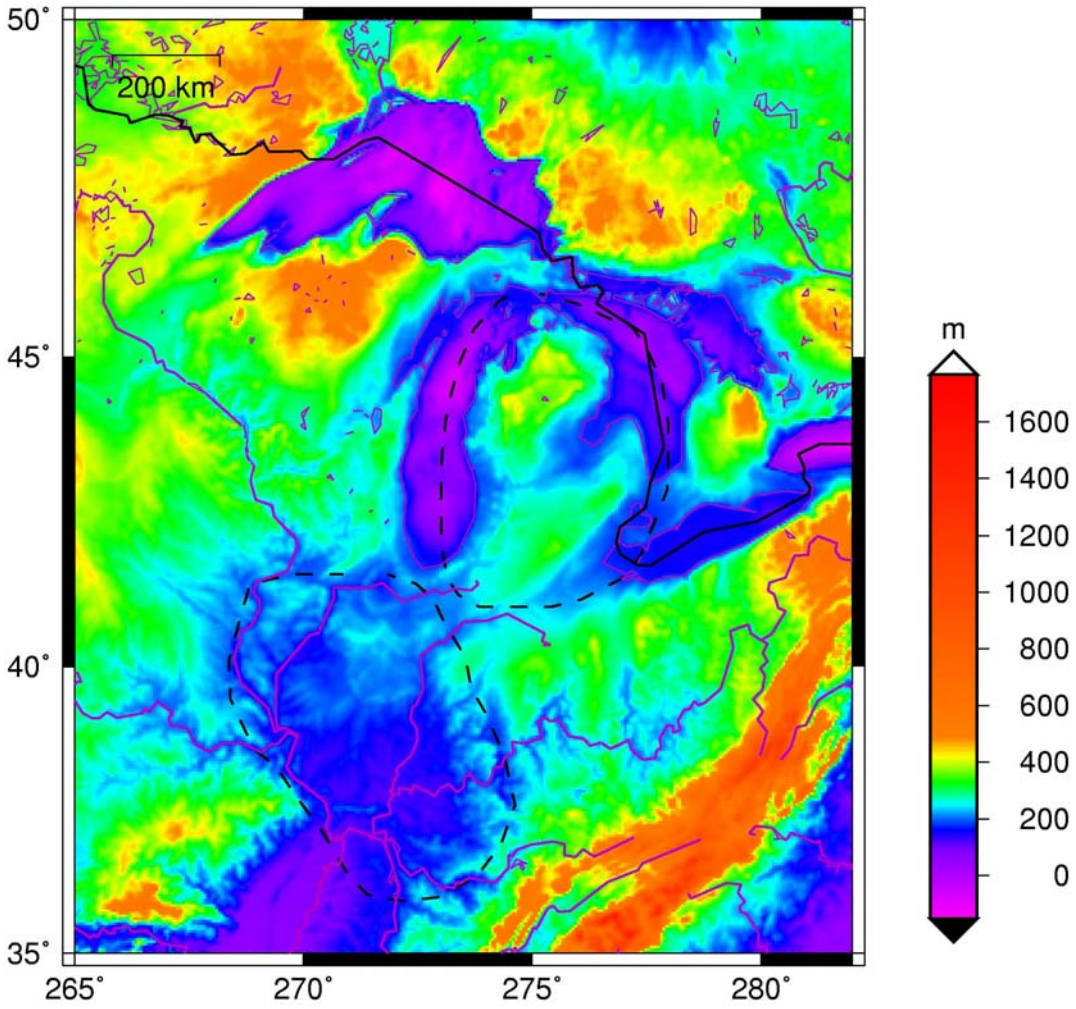

Figure 7.1.1b *Topographic map of central North America. Black: State boundaries. Blue: major rivers and coastlines (NGDC, 1 km grid)*

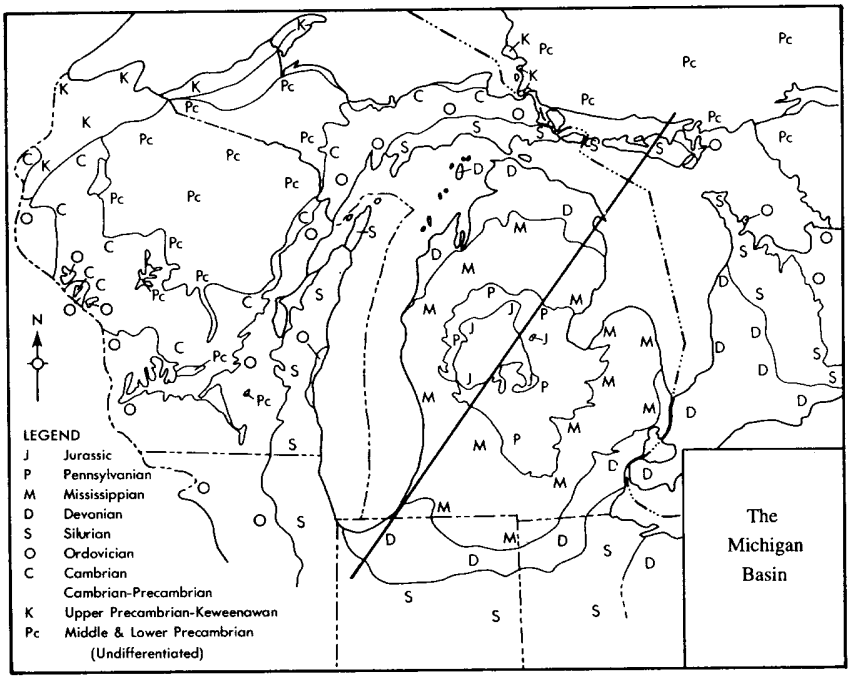

Figure 7.1.2a *Geological map of the Michigan basin (Nur and Sleep, 1984). The cross section along the marked profile is displayed in Fig. 7.1.2b.*

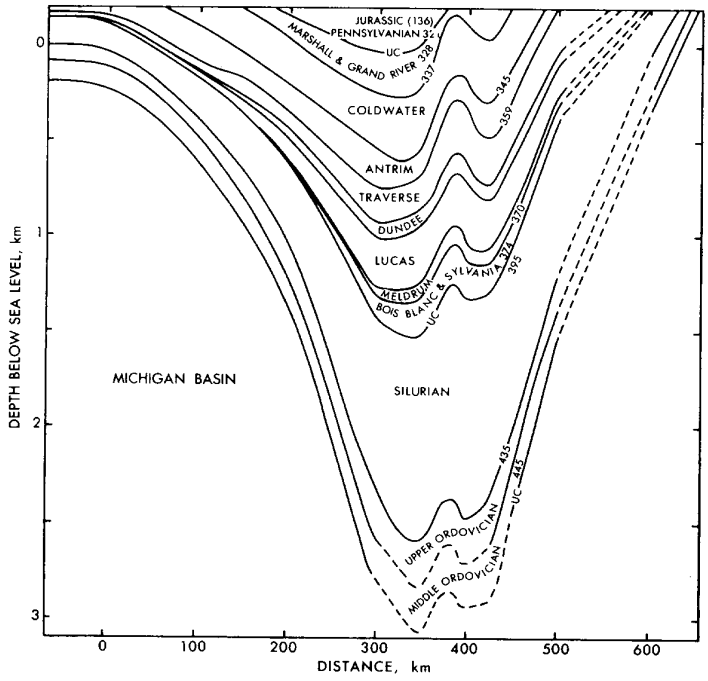

Figure 7.1.2b *Cross section through the Michigan basin (Nur and Sleep, 1984). The cross section along the profile marked in Fig. 7.1.2a.*

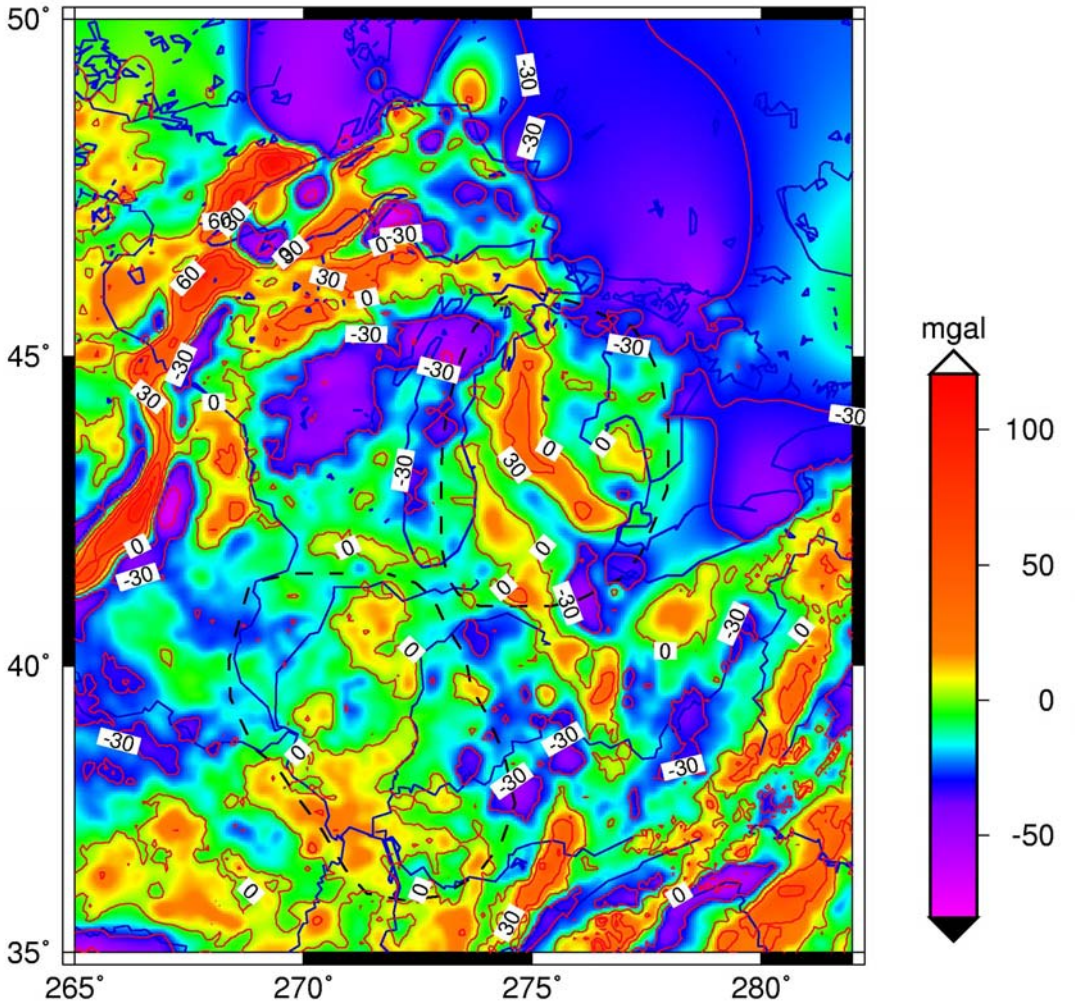

Figure 7.1.3a *Gravity anomaly (mGal) for the Michigan and Illinois basins area. (Data: BGI). Coastline and major rivers in blue. The dashed lines show the location of the basins.*

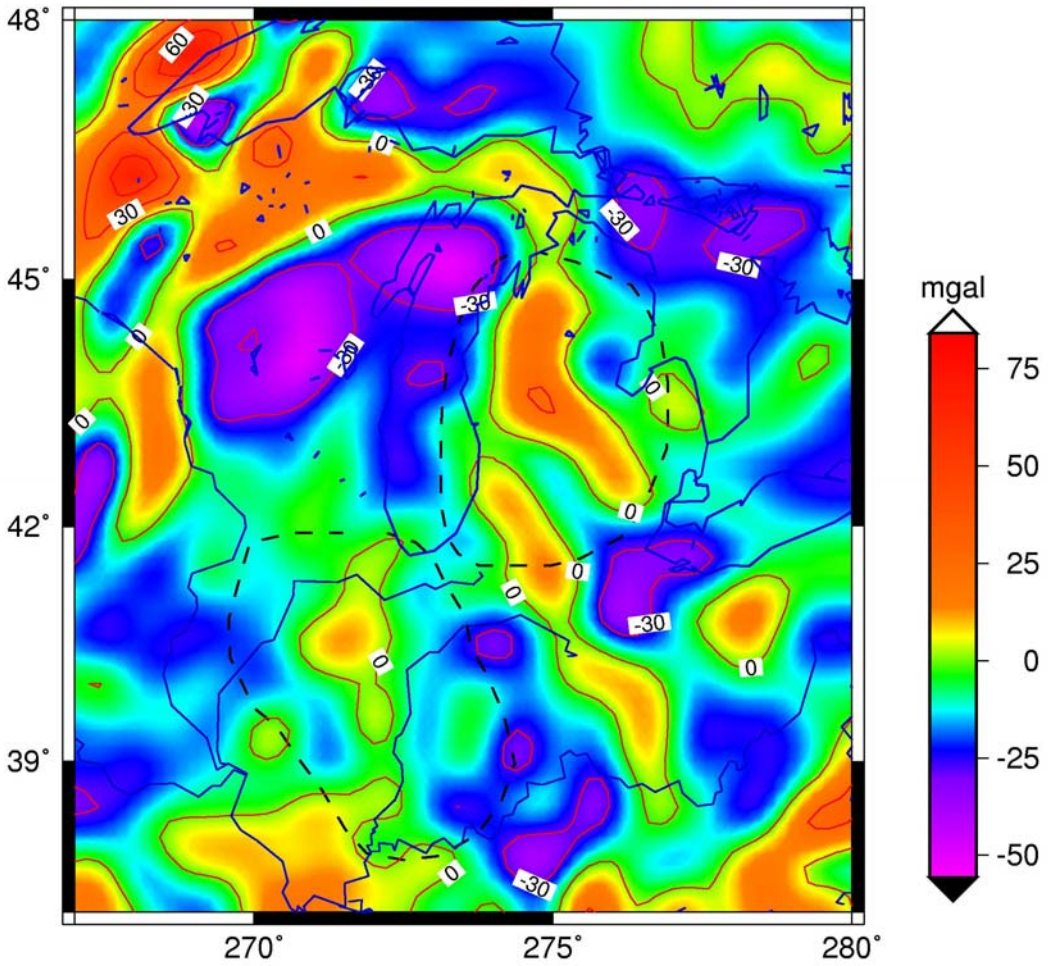

Figure 7.1.3b *Gravity anomaly (mGal) for the Michigan and Illinois basins area. (Data: EIGEN-GL04C, Förste et al., 2006). Coastline and major rivers in blue. The dashed lines show the location of the basins.*

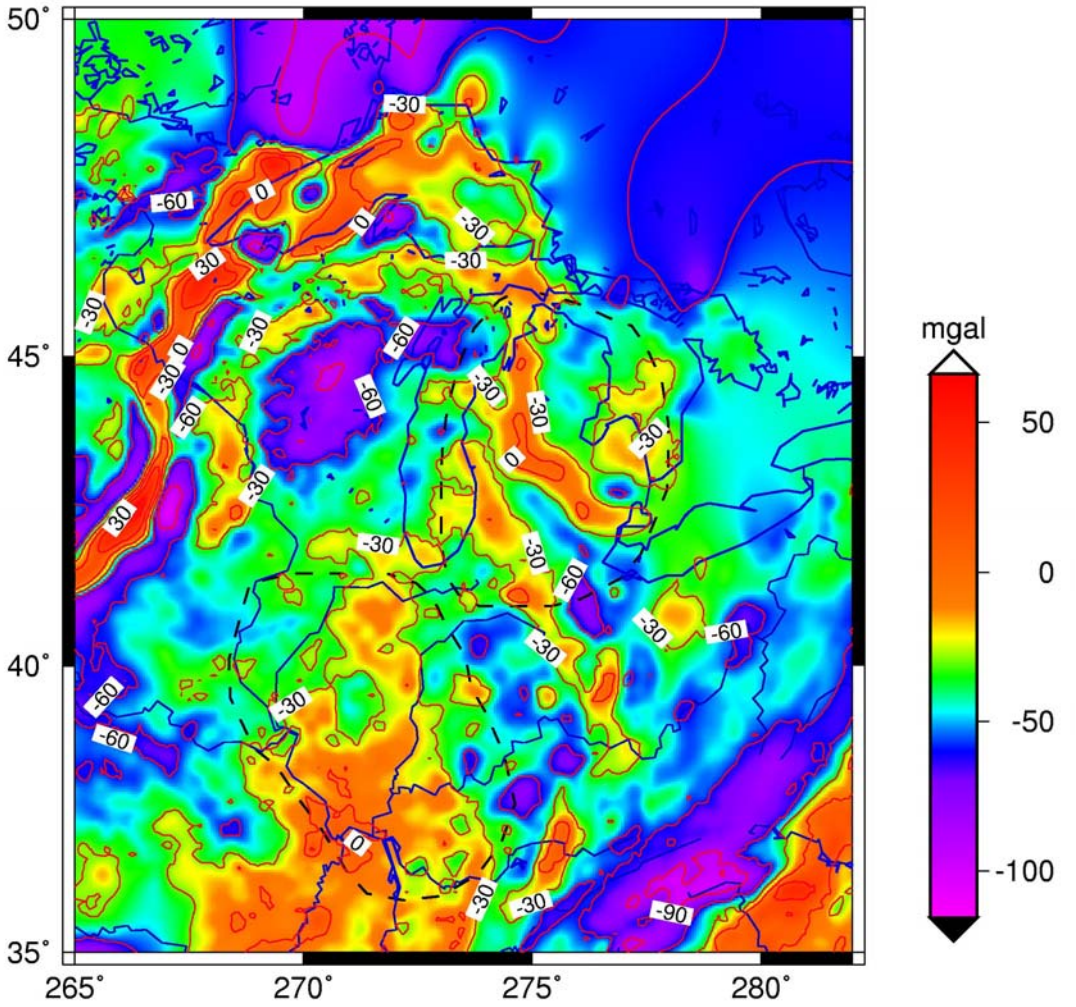

Figure 7.1.4 *Bouguer gravity anomaly (mGal) for the Michigan and Illinois basins area. (Data: BGI). Coastline and major rivers in blue. The dashed lines show the location of the basins.*

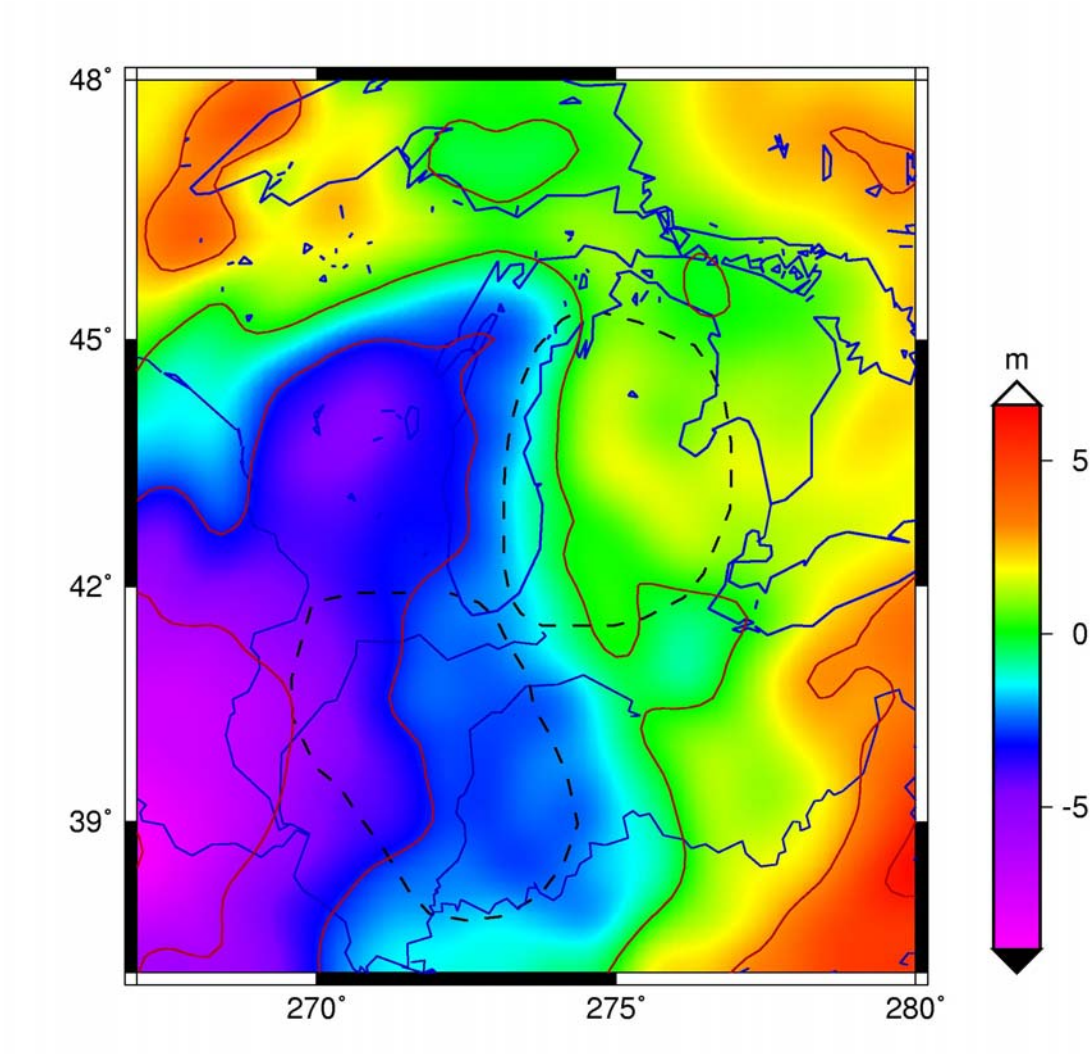

Figure 7.1.5 *Geoid residual (m) for the Michigan and Illinois basins area. Data: EIGEN-GL04C (Förste et al., 2006) freed from lowest degree and order (up to degree and order 10) harmonic components.*

7.2 Large scale sedimentary basins of South America

The South American platform counts five sedimentary depocenters, which are the Solimões, Amazon, Parnaiba, Paranà in Brazil and the Chaco-Paranà basin in Argentina (Fig. 7.2.1) (Milani and Filho, 2000; Almeida et al., 1981; Almeida et al., 2000). The basins range in size between 0.5 10^6 km^2 to over 1 10^6 km^2 and have all an elliptical to circular shape. Common to the basins is a relatively simple stratigraphic framework and the presence of large volumes of Mesozoic basaltic magma. In most of the basins, the first cycle of sediment accumulation

began during Late Ordovician. The last Paleozoic depositional cycle in all five basins terminates with Late Permian to Early Triassic deposition.

7.2.1 Solimões and Amazon basin

The Solimões basin is separated from the Amazon basin to the east by the Purus arch (see Fig. 7.2.1). The Solimões basin and the Amazon basin together extend over a length of 2500 km and width of 500 km, with the sediments reaching the thickness of up to 5000 m (Milani and Thomaz Filho, 2000). The Solimões basin covers an area of more than 0.6 10^6 km^2 with a maximum thickness of 4000 m. The sedimentary record of the Solimões basin is constituted by the Ordovician sequence, the Silurian-Devonian sequence and the Devonian-Carboniferous sequence (Fig. 7.2.2a). From Carboniferous onwards the sediments covered the barrier formed by the Purus Arch and successively the Amazon and Solimões basins became united to a single basin. A regional unconformity separates the Paleozoic record from the younger strata, consisting of the Cretaceous and Cenozoic sequences. During the Late Triassic to Early Jurassic the Paleozoic deposits have been intruded by the Penatecaua magmatics with large volumes of diabase sills and dykes (170-230 Ma).

The Amazon basin (Fig. 7.2.2b) covers an area of about 0.5 10^6 km^2, and has a thickness of up to 5000 m. The basement of the Amazon basin consists mainly of igneous and metamorphic complexes. To the east, the basin is limited by a Mesozoic rift shoulder (Gurupà arch), to the west by the Purus arch. The stratigraphy reveals the alternation of four episodes of relatively high accumulation rates (Ordovician-Early Devonian, Devonian-Early Carboniferous, Middle Carboniferous-Permian and Cretaceous to Cenozoic) succeeded by periods of low sedimentary accumulation rates (Milani and Thomaz Filho, 2000). An east-west-trending extension allowed the intrusion of magmatic bodies during Late Triassic and Early Jurassic times (Penatecaua magmatics).

7.2.2 Gravity and geoid of the Solimões and Amazon basin

The composite basin is located in a general gravity anomaly low (Fig. 7.2.3), in which a distinct positive linear feature along the central part of the basin is present. The eastern limit of the basin is formed by the Gurupà arch that emerges as a linear positive gravity feature. The western limit of the basin, formed by the Iquitos arch, emerges as a gravity high

(+30mGal). The Bouguer anomaly map (Fig. 7.2.4) also shows a chain of gravity highs of +40mGal to +90 mGal that transects the basin roughly coincident with the maximum thickness of sedimentary rocks. The gravity highs are flanked by gravity lows of -40 ± 20 mGal. The general lowering of the gravity field in correspondence of the basin is no more present in the Bouguer gravity field, pointing to a crustal thinning or in a densification of crust or upper mantle. This follows due to the fact that the sediments contribute to lower the Bouguer gravity signal. If no low is observed, there must be a Moho shallowing or else crustal densification to balance the negative signal produced by the sediments. The residual geoid (Fig. 7.2.5) shows a general geoid low, centred near to 3 degrees southward to the centre of the basin. The terrain corrected geoid (Fig. 7.2.6) correlates better to the position of the composite basin and presents a relative high of 5 m increase with respect to the northern and southern borders of the Amazon basin. The terrain corrected geoid resembles the features already observed in the gravity anomaly and in the Bouguer anomaly. Nunn and Aires (1988) model the middle Amazon basin with a flexural crustal model that includes an up to 40 km thick lower crustal body underlying the sediments and a thick crust that reaches the depth of up to 55 km. The high-density crustal body has a density of 3000 kg/m^3, with a density contrast of 150 kg/m^3 with respect to the lower crust. Tentatively, they model the shape of the basin by applying the bottom crustal load to an elastic lithosphere model of effective elastic thickness of 17.5 km. The model allows reproducing the shape of the basin reasonably well, although several discrepancies still remain. The dense crustal body is interpreted as intruded material of density intermediate to crust and mantle. The same authors suggest that the subsidence history of the Amazon has some analogies to the Michigan, Illinois and Williston basins, in the sense that the different subsidence cycles could be related to successive heating events (rifting/intrusion) followed by thermal cooling.

7.2.3 Parnaíba basin

The Parnaíba basin (Fig. 7.2.2c) occupies an area of near to 0.6 10^6 km^2 and is a circular sag with a total sedimentary section of near to 3500 m thickness in its depocenter (Milani and Thomaz Filho, 2000; Almeida et al., 1981; Almeida et al., 2000). The Ferrer-Urbano Santos arch, a positive flexural feature related to the Mesozoic opening of the equatorial Atlantic Ocean, defines the northern limit of the Parnaíba basin. Within the crystalline basement the presence of Late Proterozoic/Early Cambrian NS-trending grabens has been found (Milani and Thomaz Filho, 2000), and have been interpreted as the rift sequence that initiated the

Parnaíba basin. The Transbrasiliano fault zone cuts the eastern/southern portion of the basin and produces some structuring. This fault zone runs across the continent for 3000 km in a NE-SW trend, starting in the Equatorial Atlantic, crossing also the northernmost portion of the Paranà basin and reaching Paraguay. The stratigraphic framework contains three major Paleozoic and two Mesozoic supersequences. The older strata are mainly of Silurian age. The Devonian Supersequence is of Eifelian-Tournaisian age. The beginning of the Pennsylvanian sedimentation changes the geometry from a graben-controlled elongated to a circular configuration. The Carboniferous-Triassic supersequence follows. Two main magmatic pulses ocurred place in the basin during the Mesozoic, with intrusive emplacements and volcanic flows, the former being preferentially found in the Devonian supersequence. The first magmatic cycle, from the Triassic-Jurassic, is correlated to the Penatecuaua magmatism of the Solimões and Amazon basin and is related to the rifting of the central Atlantic. The second pulse is dated to the early Cretaceous and is related to the rifting of the South Atlantic. Between the magmatic pulses there is Jurassic sedimentation, followed by the Cretaceous supersequence.

7.2.4 Gravity and geoid for the Parnaiba basin

The gravity anomaly (Fig. 7.2.7) over the Parnaiba basin is a well-developed minimum (-10 to -45 mGal), with the higher values pertaining to the centre of the basin, where the sediment thickness should be the greatest. It is interesting to note, that the gravity anomaly forms a concentric pattern, with less negative values in the centre (lowest values along a concentric ring) and intermediate negative values inboard of the basin margin. This could be an indication of the flexural response of the crustal thickness variation, which in the centre of the basin is closest to the locally compensated isostatic equilibrium. The Bouguer anomaly (Fig. 7.2.8) is nearly uniform in the basin with a value of near to -50 mGal, and is characterized by an increase (to -25 mGal) along the border of the basin. The southernmost part of the basin forms an exception to this picture, and has more negative Bouguer anomaly values near to -80 mGal. The northern border marked by the Ferrer-Urbano Santos arch is delineated by a relative gravity high of -25 mGal. The geoid field (Fig. 7.2.9) as well as the terrain corrected geoid (Fig. 7.2.10) do not show evident features correlated to the basin. Only along the eastern border of the basin the geoid shows a broad increase, located on the eastern geographical protuberance of the South-American continent.

7.2.5 Paranà Basin

The Paranà basin is located in southeastern Brazil and extends into Uruguay, Argentina and Paraguay (Fig. 7.2.1). This large intracratonic basin covers an area of about 1.100.000 km^2 and is bordered in its northwestern, northeastern and southern sector by the cratonic areas of Amazonia, Sao Francisco and Rio della Plata, respectively. To the east the basin is limited by the Atlantic continental margin. To the south the basin borders with the Chaco-Paranà basin, this last one covering an area of close to 500 000 km^2. The Paranà basin is filled with sedimentary and volcanic rocks that range in age from Ordovician to Cretaceous with a maximum thickness about 5.5 km (Milani and Ramos, 1998) (Fig. 7.2.2d). The Paranà basin is set on those areas of the South-America platform which were affected by the metamorphic and magmatic event of the Brazilian cycle (ca.700—450 m.y.). The crystalline basement is assumed to have formed by a Proterozoic cratonic nucleus surrounded by mobile belts as inferred from radiometric dates from two basement samples (Cordani et al., 1984).

Basin development started in the early Paleozoic and the initial Ordovician subsidence is dated to 440 Ma. Another important subsidence stage occurred in Carboniferous-Permian times (starting about 296 Ma). Extensive flood basalts were extruded in most of the basin from 137 Ma to 130 Ma, just prior to the beginning of the rifting in the South Atlantic. The basalt layers (Serral Geral formation and Gondwana III supersequence) reach a maximum thickness of around 1.5 km near the basin centre. The basin subsidence continued until Cretaceous times, with the Bauru sediments (300 m) overlying the basalts (An & Assumpção 2006).

Average crustal thickness in the Paranà basin was estimated to be approximately 42 km, thicker than for the topographic elevated areas of the Brasilia belt and Sao Francisco Craton (Assumpção et al., 2002). From isostatic considerations and by observing the gravity field a lower crust or upper mantle with higher densities can be expected. The recent work of An & Assumpção (2006) on the S-wave velocity below the basin (average velocities lower than 3.8 km/s and normal Vp/Vs ratios around 1.73) exclude the presence of a high-density lower crust, pointing to high-density material in the upper, lithospheric mantle that is correlating with an increase of seismic velocity as observed from Rayleigh wave studies at a depth of 100-150 km (Feng et al., 2004).

7.2.6 Gravity and geoid in the Paranà basin

The Paranà basin is outlined by a gravity anomaly low (Fig. 7.2.11) of more than -30mGal, flanked by a gravity high (up to +30 mGal). Along the central part of the basin a relative N-S trending gravity high is found that separates the basin into two sub-areas. In the Bouguer anomaly (Fig. 7.2.12) a broad low is found to the NE of the basin in correspondence of the fold-belt bordering the San Francisco craton. The basin is outlined by a definite low with values between -60 and –90 mGal. Again a linear relative gravity high along the central part of the basin, in correspondence with the maximum thickness of the sediments is found. The basin is bordered to the SE by an increase of Bouguer gravity, corresponding to the Ponta Grossa arch (dykes). Also along the entire western margin the basin outline is accompanied by a Bouguer gravity increase. The Moho lies at a depth of 40-45 km and cannot explain the gravity variations across the basin, as the variations are too small. The gravity signal thus must be due to density variations in the upper mantle, as the results of An & Assumpção (2006) exclude the presence of a high-density body in the lower crust along the central basin axis. The basin is well outlined also by the geoid undulations (Fig. 7.2.13), which show a relative decrease of 10 m from the basin margins to centre. The terrain-reduced geoid (Fig. 7.2.14) also features an increase of values along the central axis of the basin, in correlation with an increased Bouguer anomaly. The fact that the increase in values is found both in gravity and the geoid points to a deep source of the signal.

7.2.7 Comparison to West Siberian and East Barents Sea

The composite Amazon-Solimões basin has some features in common to the West Siberian basin, what concerns the position of the linear gravity high with respect to the sediment thickness. The linear gravity and geoid high which is found in the Amazon basin is analogous to the N-S trending gravity high flanked by gravity lows found in the West Siberian basin, and has a stronger expression in the northern section of the basin. The linear gravity high can be traced without interruptions farther south as well. This would also imply the presence of a high-density lower crustal body below the Western Siberian basin.

The Paranà basin differs in one important aspect from the other basins in this study: the flood basalts cover nearly 2/3 of the basin, implying that the greater part of the sediment-isopachs is below the basalts. In the Western Siberian, the Michigan basin, and probably the Tarim basin

and east Siberian, the volcanism precedes the greater part of the basin deposition. This is an important aspect to consider for the thermal evolution of the basin. Common to the East Barents Sea and the Michigan basin is the inferred high-density upper mantle and the anomalous isostatic compensation.

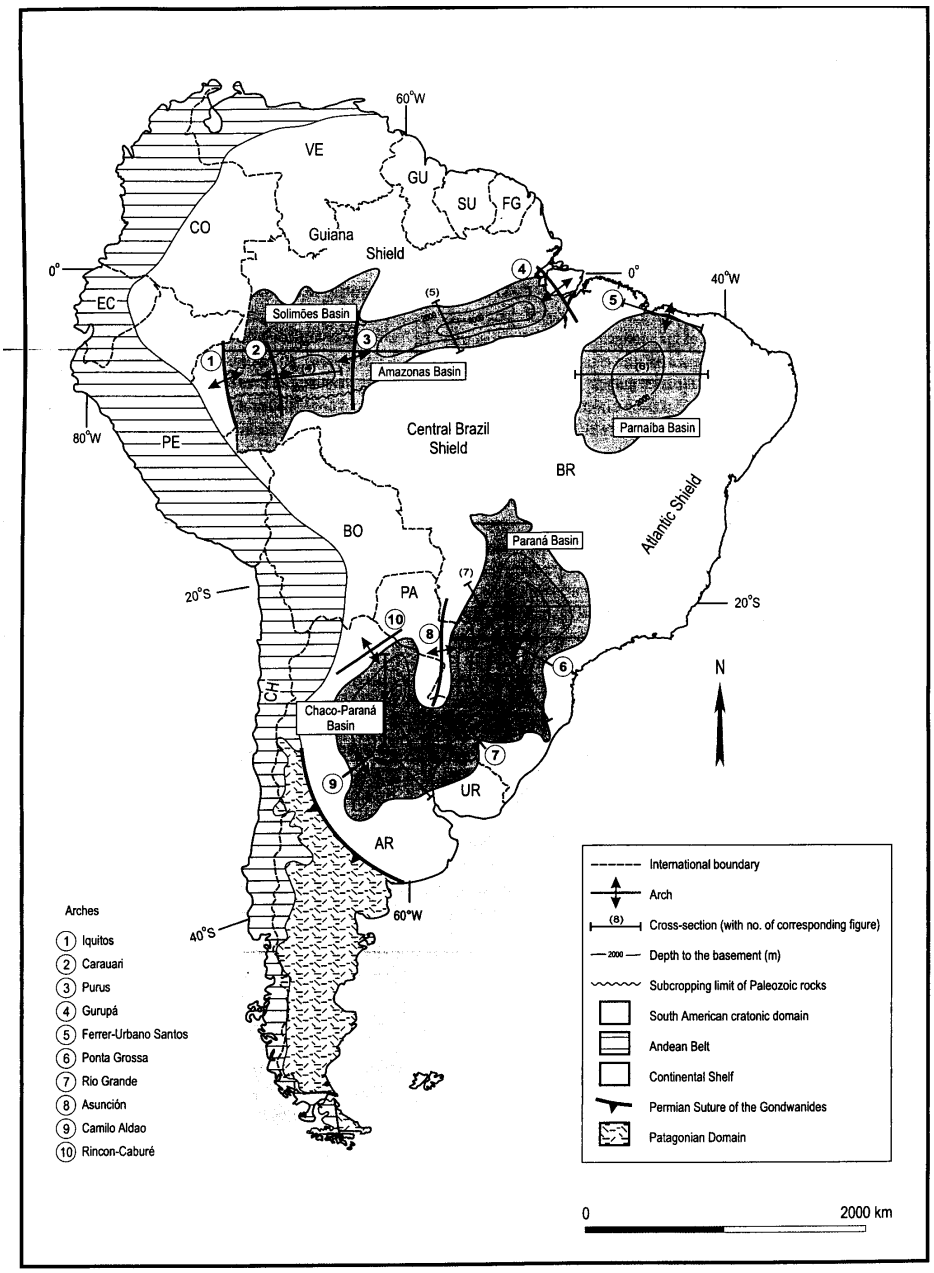

Figure 7.2.1a *Large scale basins of the South American platform (Milani and Thomaz Filho, 2000).*

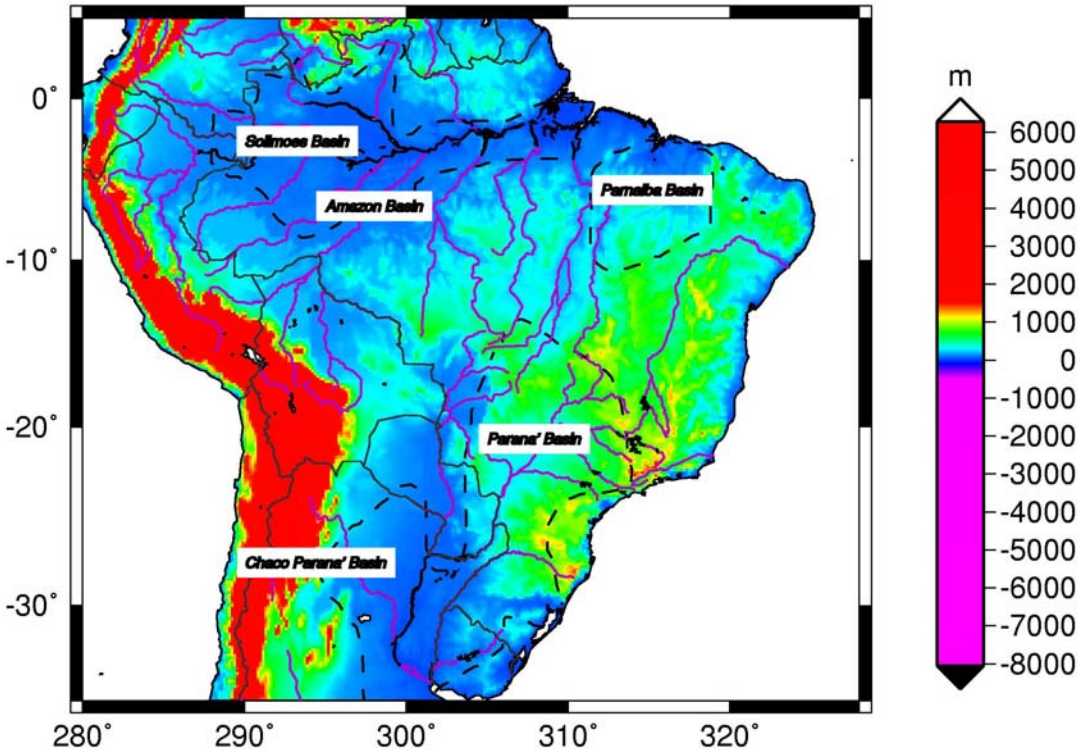

Figure 7.2.1b *Topography and the large scale basins of the South American platform (basin outline after Milani and Thomaz Filho, 2000). Rivers: purple. Coastline: black. State borders: grey.*

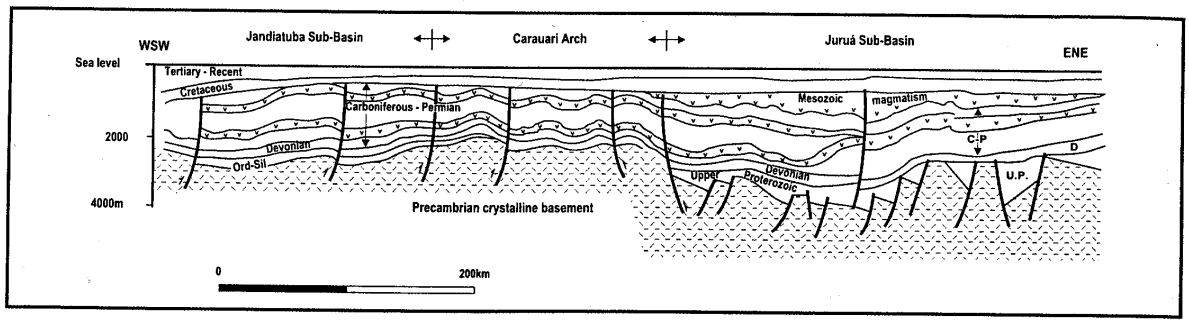

Figure 7.2.2a **Cross section of the Solimoes basin (Milani and Thomaz Filho, 2000).**

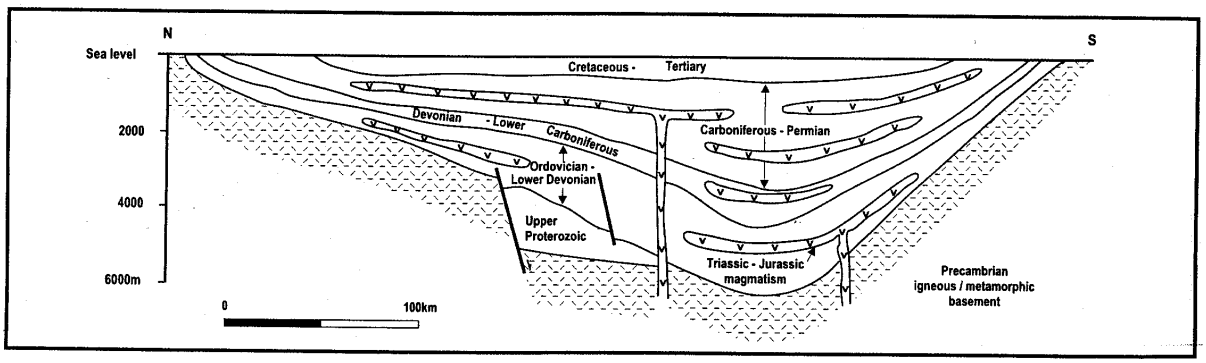

Figure 7.2.2b *Cross section of the Amazon basin (Milani and Thomaz Filho, 2000).*

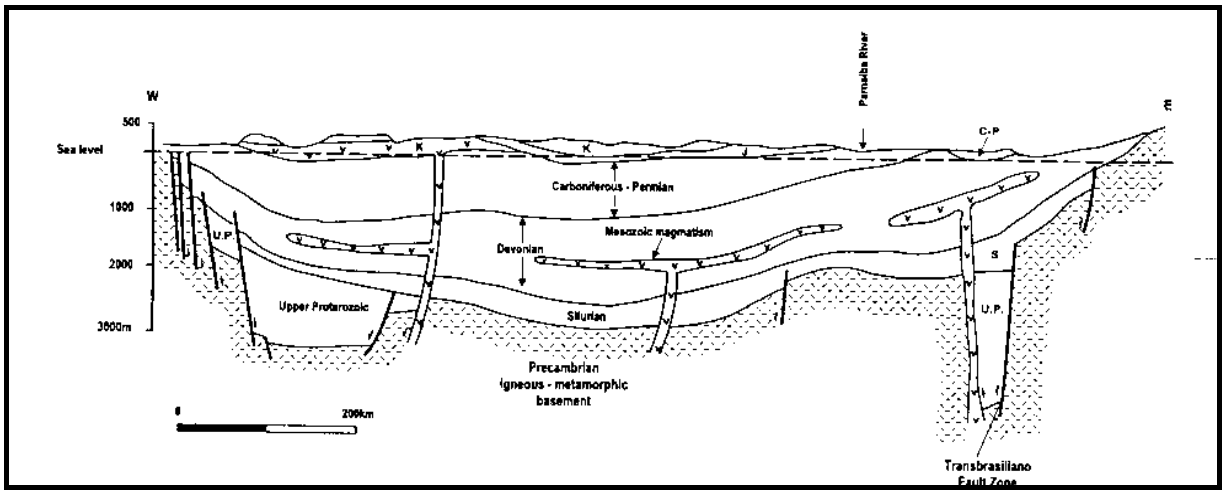

Figure 7.2.2c *Cross section of the Parnaiba basin (Milani and Thomaz Filho, 2000).*

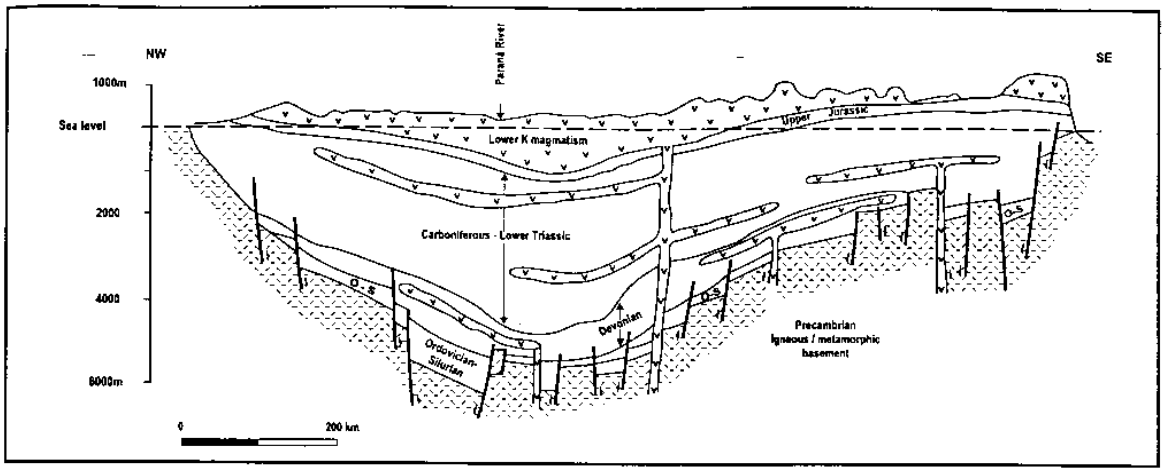

Figure 7.2.2d *Cross section of the Paranà basin (Milani and Thomaz Filho, 2000).*

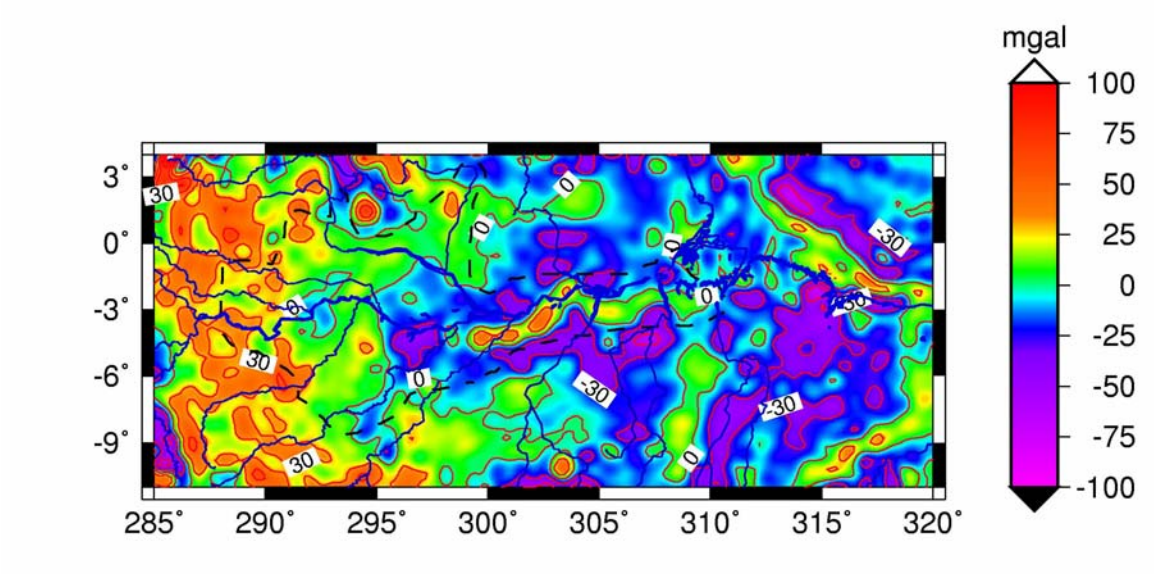

Figure 7.2.3 *Gravity anomaly for the Solimões and Amazon basins (data: EIGEN-GL04C, Förste et al., 2006). Coastline and major rivers in blue.*

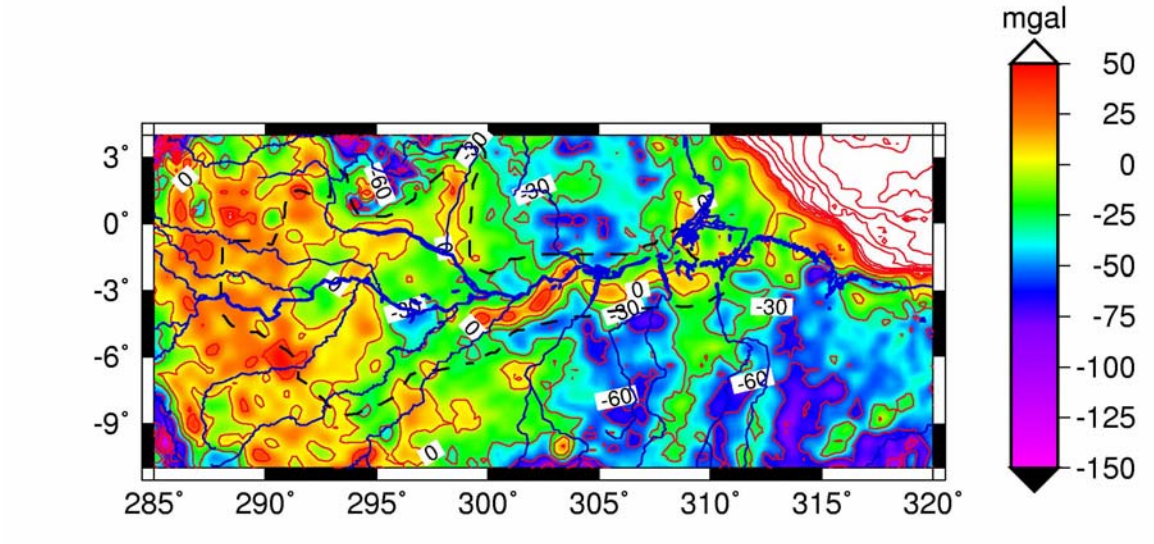

Figure 7.2.4 *Bouguer anomaly (mGal) for the Solimões and Amazon basins. Data: EIGEN-GL04C (Förste et al., 2006).*

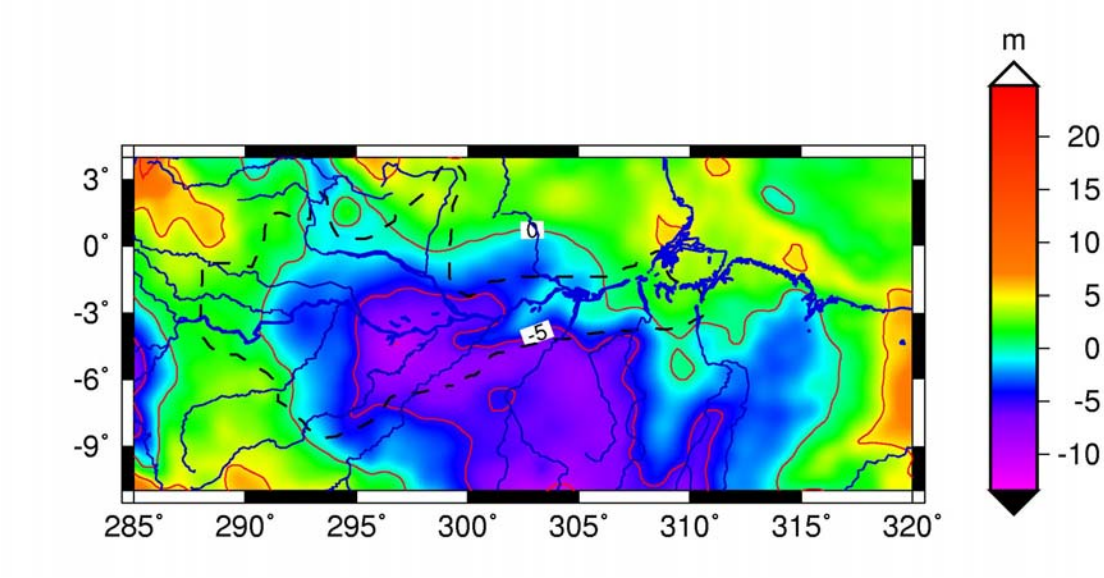

Figure 7.2.5 *Geoid residual (m) for the Solimões and Amazon basins. Data: EIGEN-GL04C (Förste et al., 2006) freed from lowest degree and order (up to degree and order 10) harmonic components.*

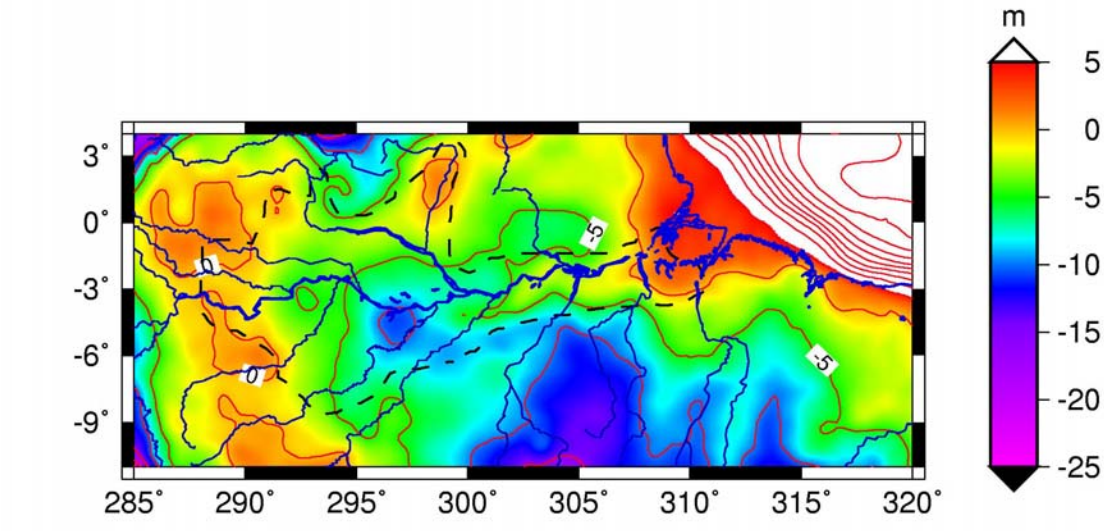

Figure 7.2.6 *Terrain corrected Geoid residual (m) for the Solimões and Amazon basins. Data: EIGEN-GL04C (Förste et al., 2006) freed from lowest degree and order (up to degree and order 10) harmonic components.*

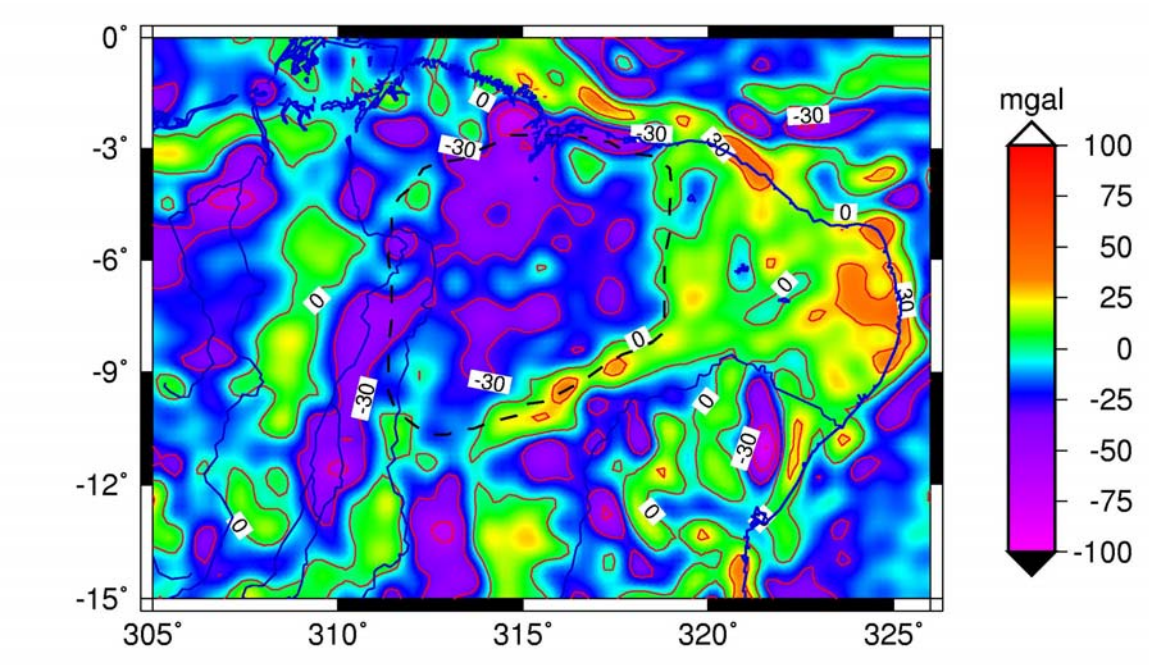

Figure 7.2.7 *Gravity anomaly for the Parnaiba basin (data: EIGEN-GL04C, Förste et al., 2006). Coastline and major rivers in blue.*

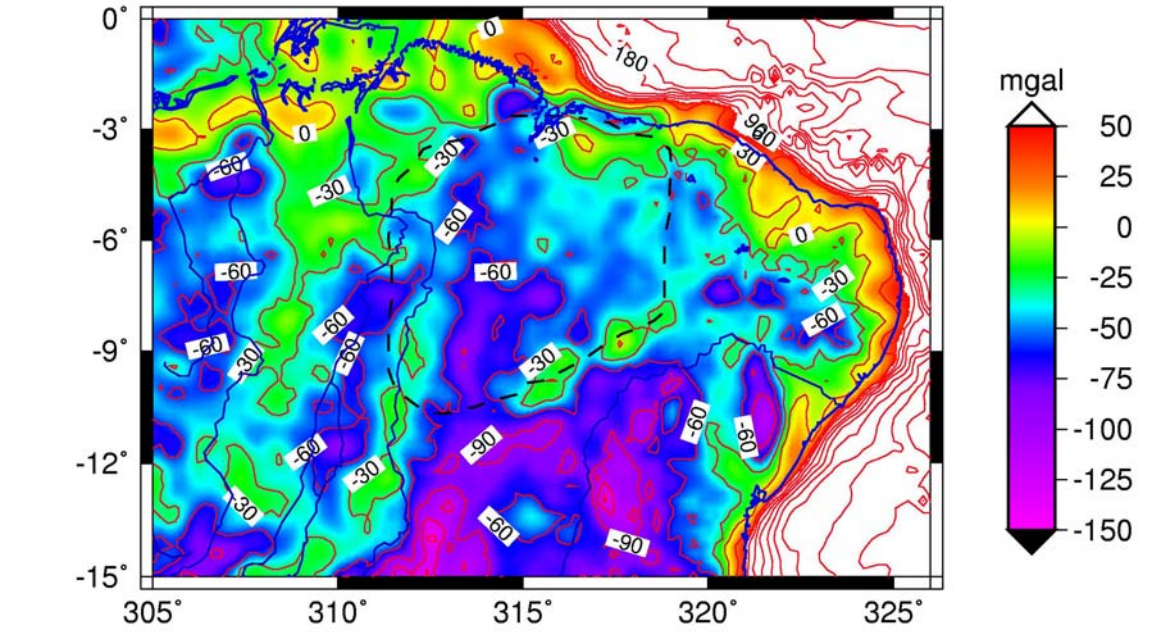

Figure 7.2.9 *Bouguer anomaly (mGal) for the Parnaiba basin. Data: EIGEN-GL04C (Förste et al., 2006).*

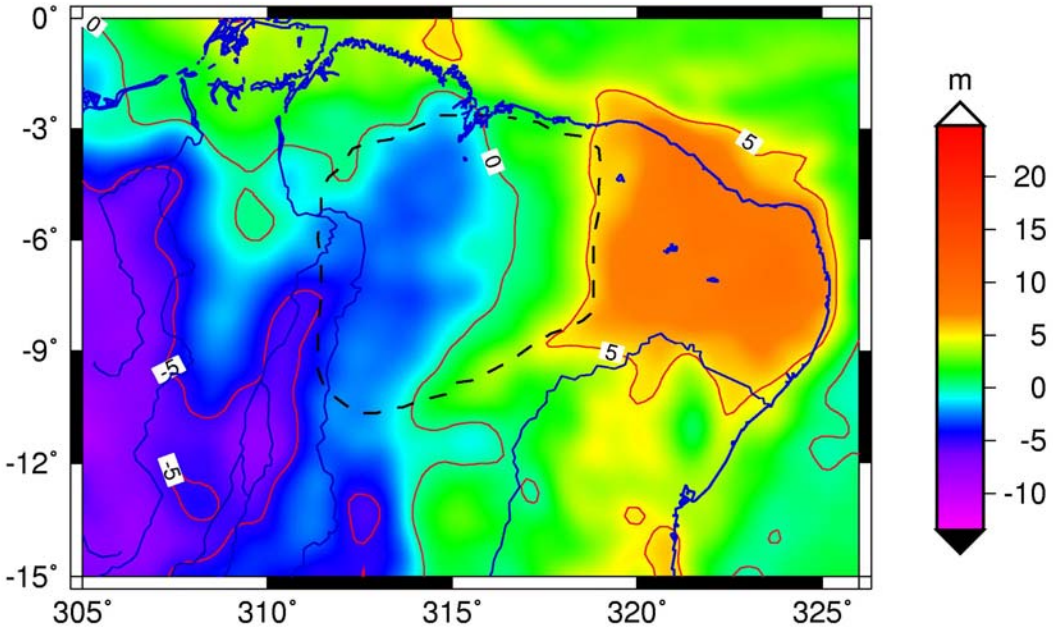

Figure 7.2.10 *Geoid residual (m) for the Parnaiba basin. Data: EIGEN-GL04C (Förste et al., 2006) freed from lowest degree and order (up to degree and order 10) harmonic components.*

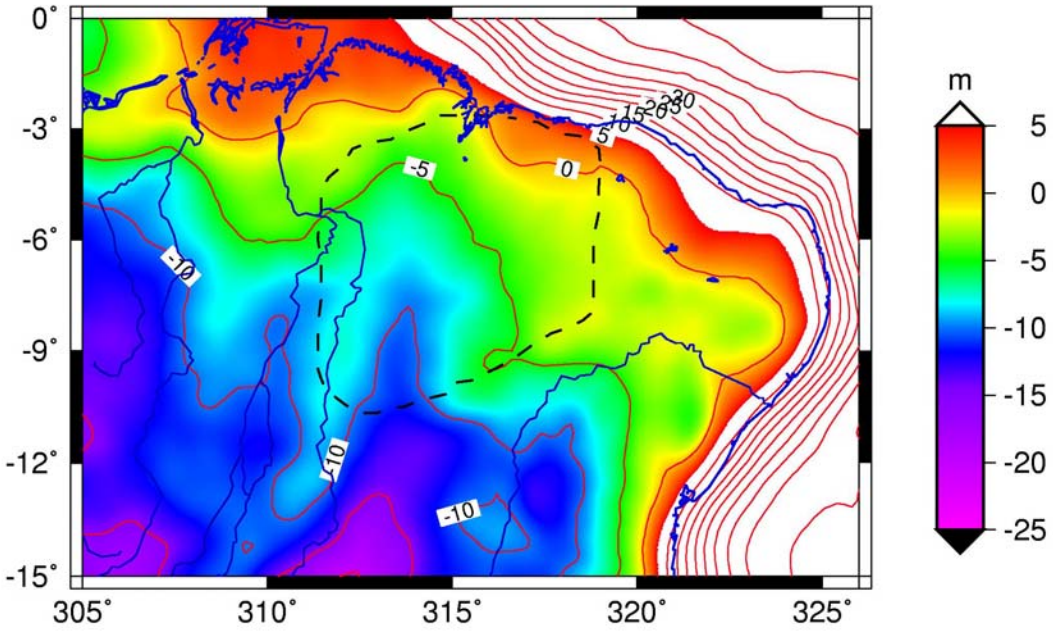

Figure 7.2.10 *Terrain corrected Geoid residual (m) for the Parnaiba basin. Data: EIGEN-GL04C (Förste et al., 2006) freed from lowest degree and order (up to degree and order 10) harmonic components.*

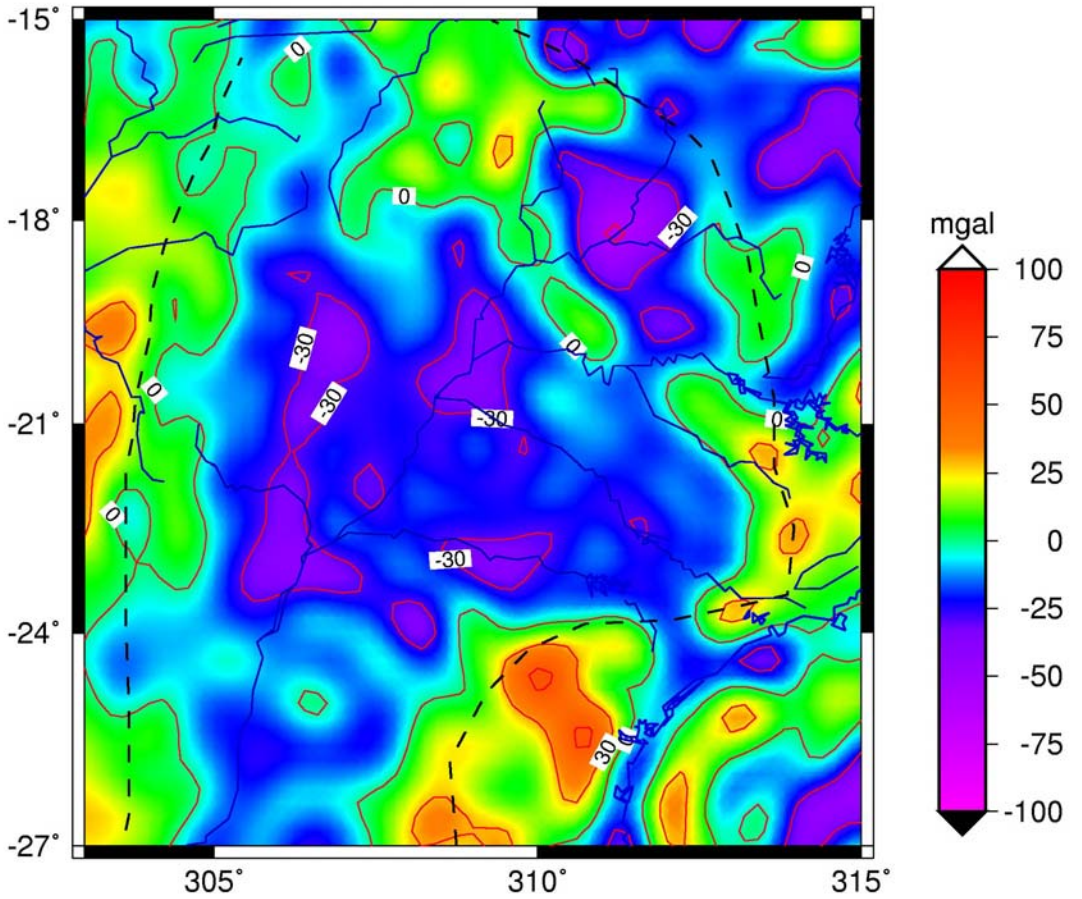

Figure 7.2.11 *Gravity anomaly for the Paranà basin (data: EIGEN-GL04C, Förste et al., 2006). Coastline and major rivers in blue.*

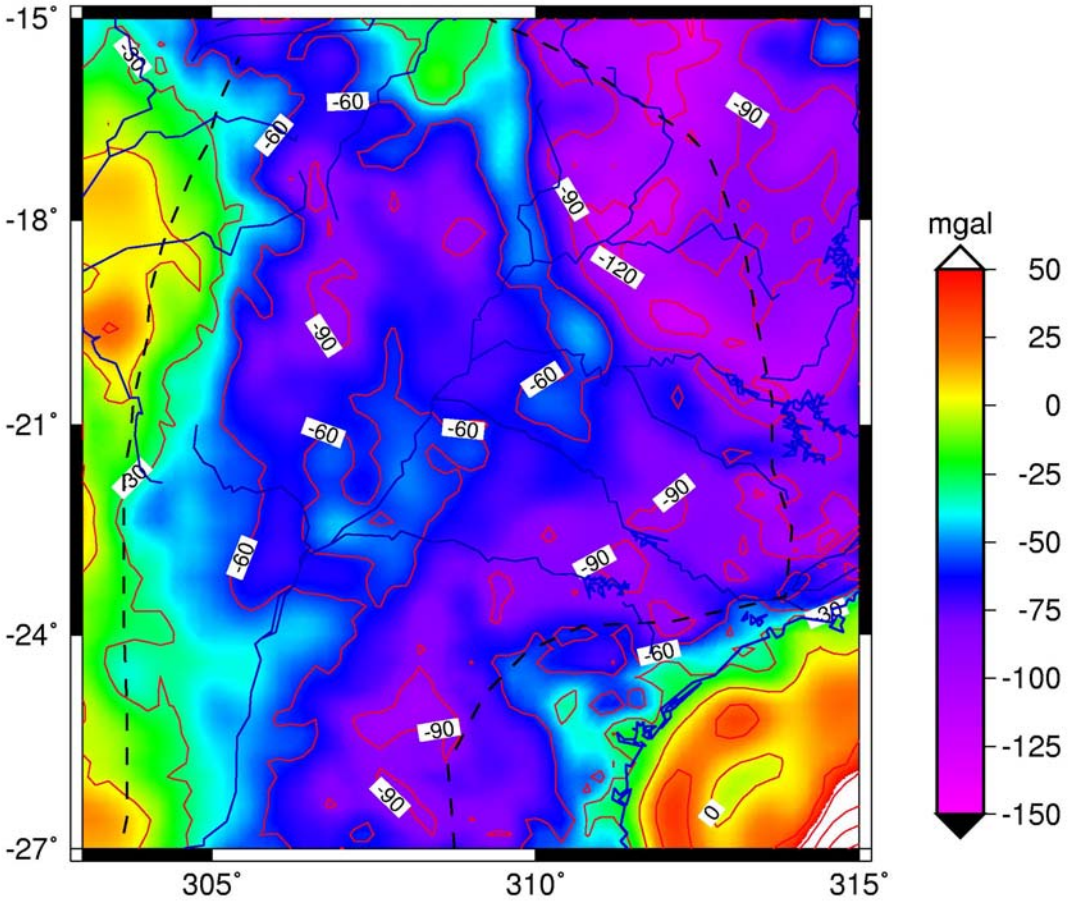

Figure 7.2.12 *Bouguer anomaly (mGal) for the Paranà basin. Data: EIGEN-GL04C (Förste et al., 2006).*

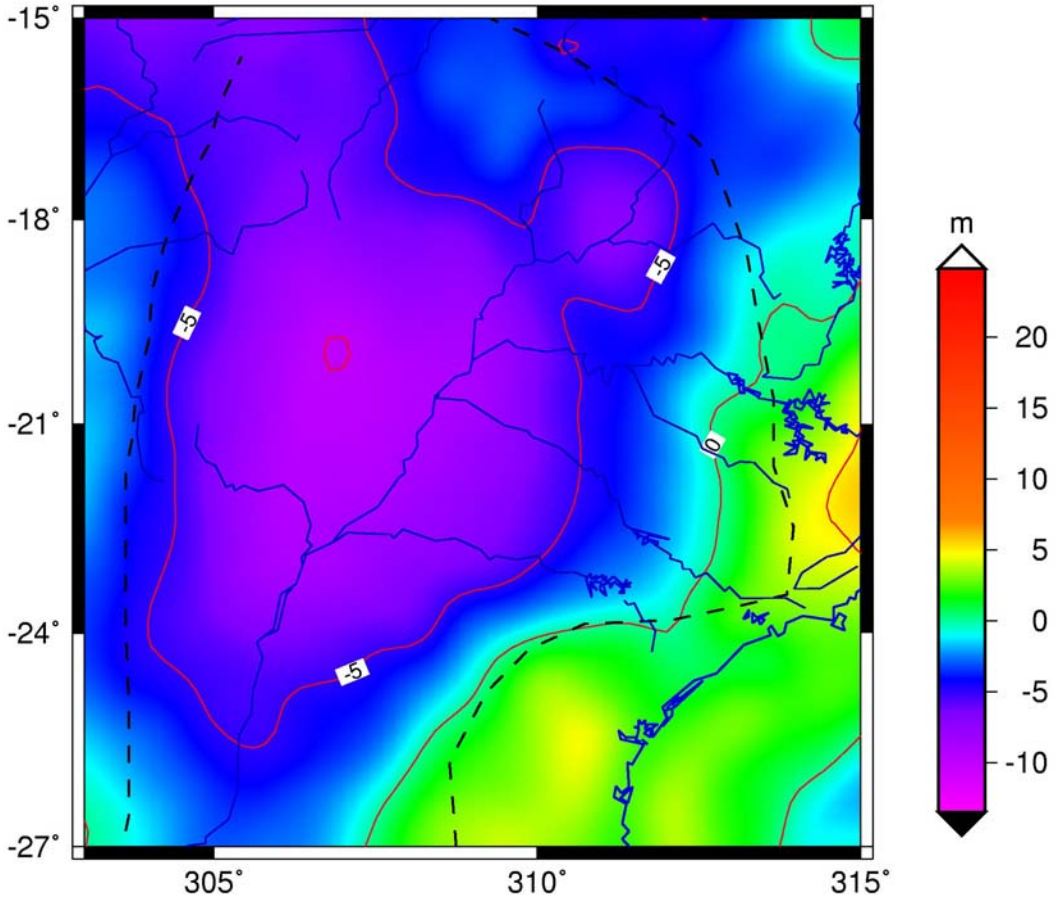

Figure 7.2.13 *Geoid residual (m) for the Paranà basin. Data: EIGEN-GL04C (Förste et al., 2006) freed from lowest degree and order (up to degree and order 10) harmonic components.*

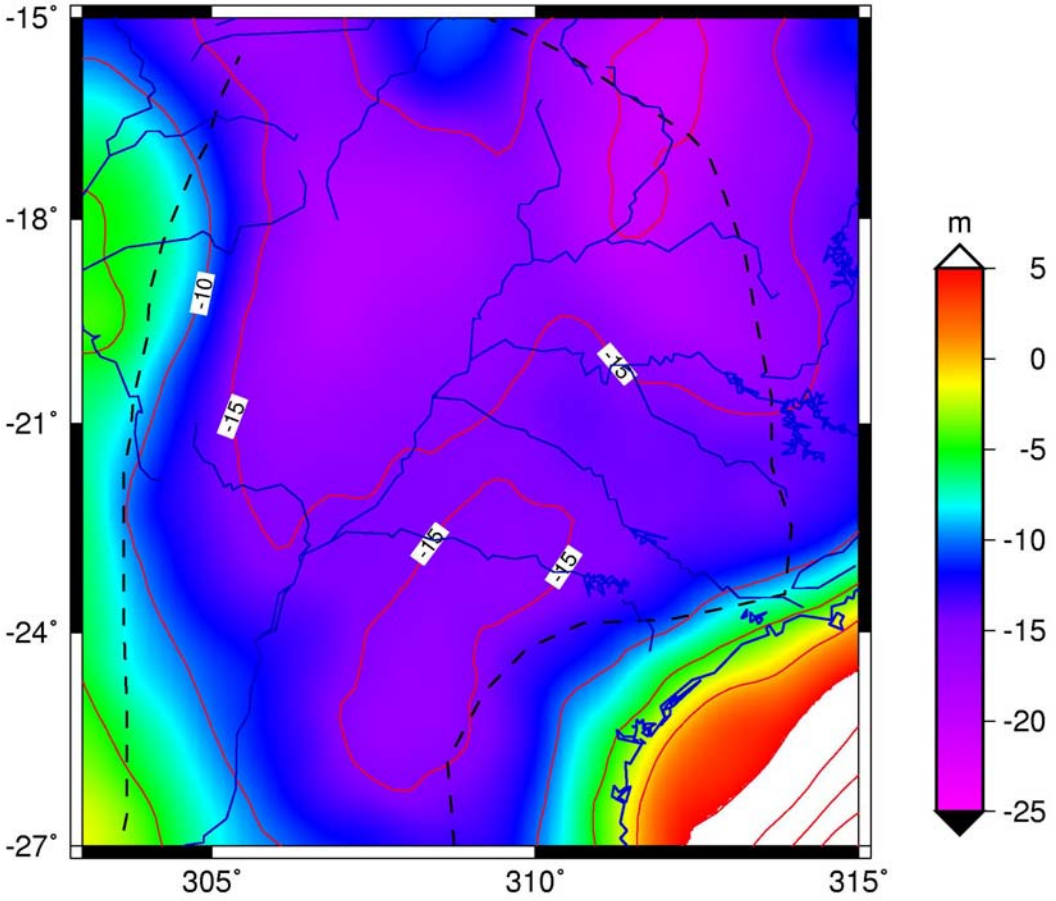

Figure 7.2.14 *Terrain corrected Geoid residual (m) for the Paranà basin. Data: EIGEN-GL04C (Förste et al., 2006) freed from lowest degree and order (up to degree and order 10) harmonic components.*

7.3 Tarim Basin

The Tarim basin lies in the southern Xinjiang province, in northwest China, and is surrounded by the Kunlun, Tien Shan and Altyntagh mountains to the south, north and southeast, respectively (Fig. 7.3.1a and b). The Tarim basin extendss over an area of near to 0.8 $x10^6$ km^2, calculation based on the sediment isopach map furnished by the Institute of Geodesy and Geophysics, Chinese Academy of Sciences (Lithospheric dynamic Atlas, 1989). The Precambrian to Phanerozoic strata locally exceed the thickness of 15 km (Yuzhu and Zhihong, 1996; Jia et al., 1998; Guo et al., 2005). The Cenozoic basin evolution is influenced by uplift and erosion of the surrounding mountains (Sobel et al., 2003). The Carboniferous to Permian sequence of the Tarim is believed to be mostly complete and comparable with that of the Urals-Russian platform and central Asia basins (Chen and Shi, 2003). Tectonically, the Tarim basin is separated to the south from the Kunlun fold belt by the Kunlun Mountain frontal suture and the Altyn Tagh deep fault; to the north it is separated from the Tien Shan fold belt and the Turpan-Hami basin by the southern Tien Shan suture and the northern Kurugtagh fault. The basin has a long geologic history, spanning from the Proterozoic to the Quaternary. The basin comprises an east-west central uplift zone (Bachu uplift) that divides the basin into two depressions during the Carboniferous and Permian. The Permian sedimentary section includes a volcanic unit that comprises basalt, tuffaceous silty mudstone with a thickness of more than 300 m. The basalt layer has been found in large areas of the basin in boreholes at a variable depth of 3000 to over 5000 m. The age of the unit has been inferred to be Wordian-Capitanian (Mid-upper Permian) (Chen and Shi, 2003).

7.3.1 Gravity and geoid in the Tarim basin

The gravity anomaly (Fig. 7.3.2) of the Tarim basin is in general very negative, between -100 and -180 mGal. The Western Tarim basin has a linear gravity high, which may be connected to uplift in the basement (Bachu uplift: Sobel et al., 2003). The negative basin-anomalies form a negative-positive couple with surrounding high mountain ranges, which comprise the Tian Shan (North) and the Kun Lun (South). The positive negative couple, which aligns the steep topographic change, is typical for a topography related to flexure. The strong negative anomalies over the basin show that it is not in isostatic equilibrium according to Airy-type isostasy. The Bouguer anomaly (Fig. 7.3.3) is also strongly negative, varying between -100

and -200 mGal, with a sedimentary contribution to the gravity field in the order of -100 mGal (Braitenberg et al., 2003). Here, the Bachu uplift is clearly seen in the Bouguer field. The geoid field (Fig. 7.3.4) is between -10 and -20 m, and correlates with the basin extension. The terrain corrected Geoid (Fig. 7.3.5) shows a relative geoid high throughout the basin. The Qaidam basin does not emerge as a localised anomaly, as it does for the gravity field. According to a 1°x1° Moho model from the database of the Chinese Academy of Sciences, Institute of Geodesy and Geophysics, the basin is underlain by a 45 km deep Moho, which deepens towards the northern, eastern and southern margins of the basin.

7.3.2 Comparison to West Siberian and East Barents Sea

The Tarim basin has in common with the West Siberian basin the presence of the extensive basalt strata of Permian age. As in the West Siberian Basin, Mesozoic to Cenozoic sedimentation brought the basalt layer to great depth (in the WSB up to 6000 m, in the Tarim basin up to 5000 m). The depth ranges of the basement are similar for the Tarim and West Siberian basin. The Tarim basin has a very significant geoid and gravity anomaly, which are both highly negative. There is a marked difference in the geoid and gravity signal with respect to the West Siberian basin, which has a Bouguer anomaly more positive than –50 mGal and positive values of the geoid. This points to a very different structure in the crustal column and maybe also in the upper mantle densities.

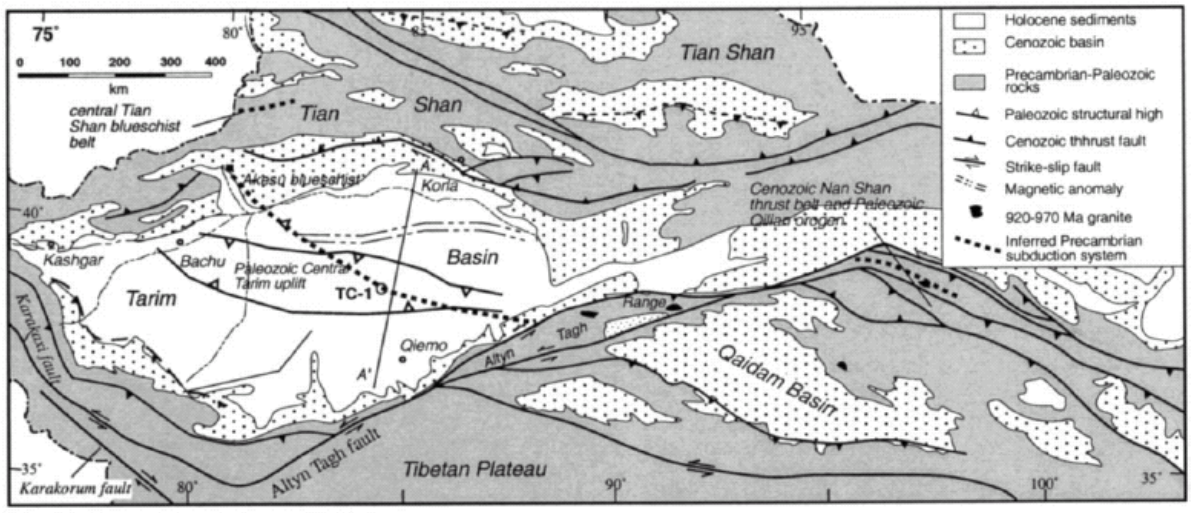

Figure 7.3.1a *Simplified tectonic map of the Tarim basin and its surrounding areas in northwest China TC-1: Central Tarim Geologic Survey Well (from Guo et al., 2005).*

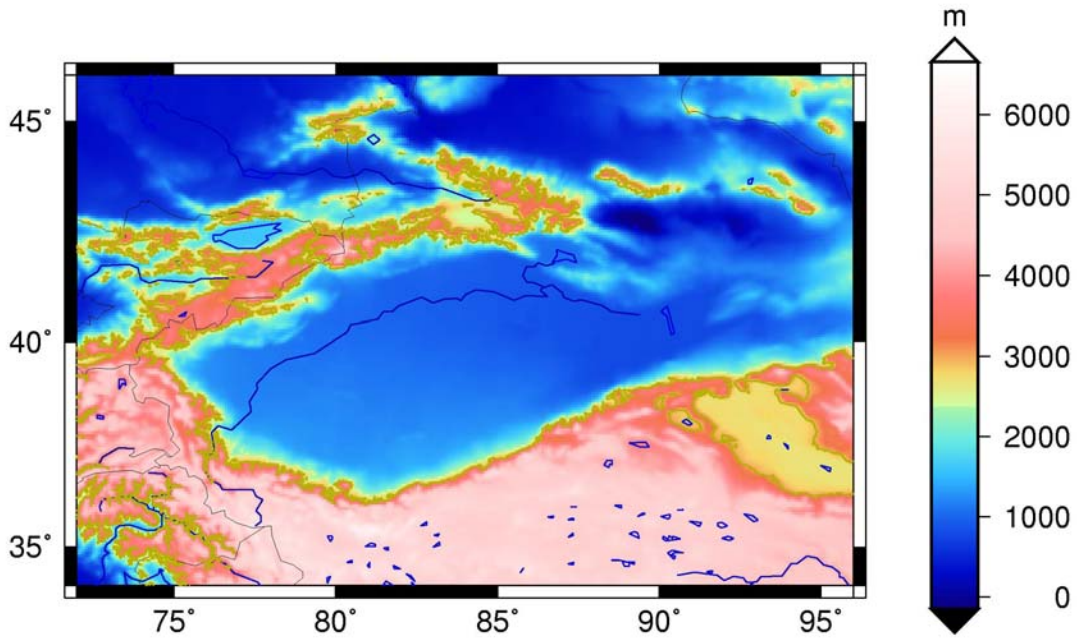

Figure 7.3.1b *Topography (m) for the Tarim basin.*

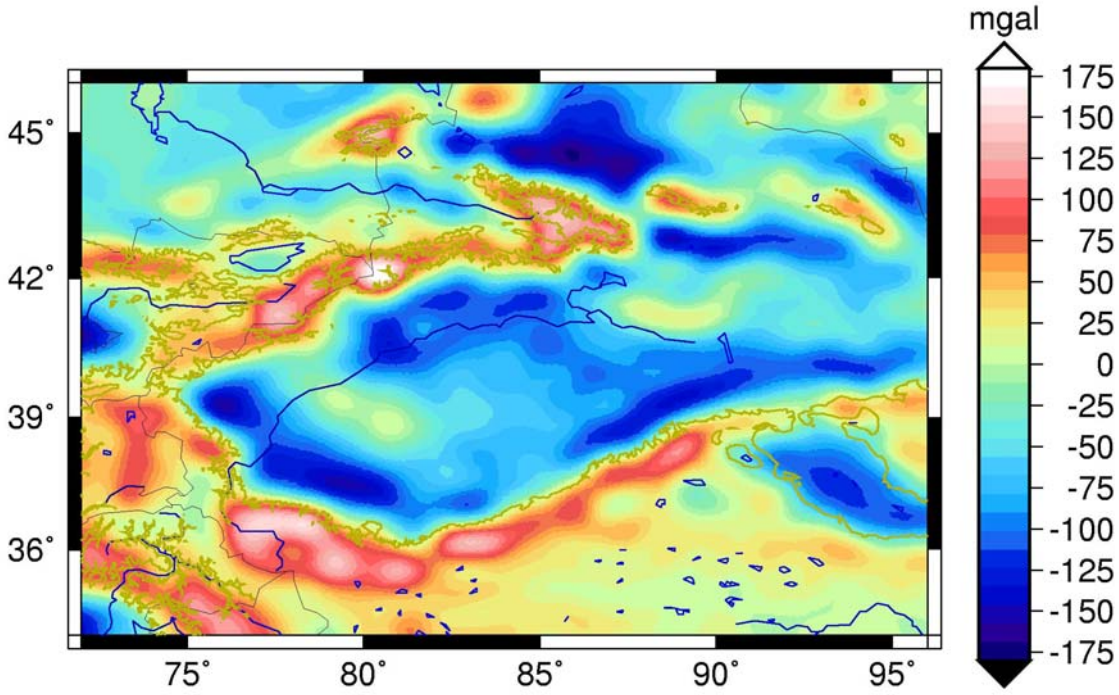

Figure 7.3.2 *Gravity anomaly for the Tarim basin (data: EIGEN-GL04C, Förste et al., 2006). Coastline and major rivers in blue. The Tarim basin is characterised by a strong gravity minimum also found for the Qaidam basin.*

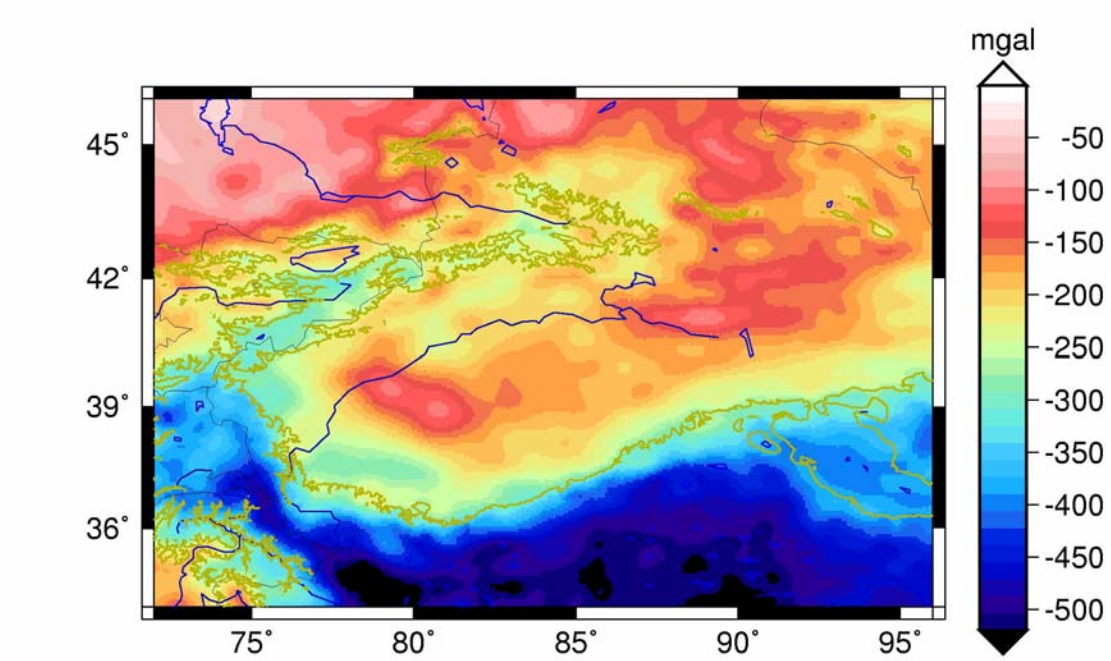

Figure 7.3.3 *Bouguer anomaly (mGal) for the Tarim basin. Data: EIGEN-GL04C (Förste et al., 2006).*

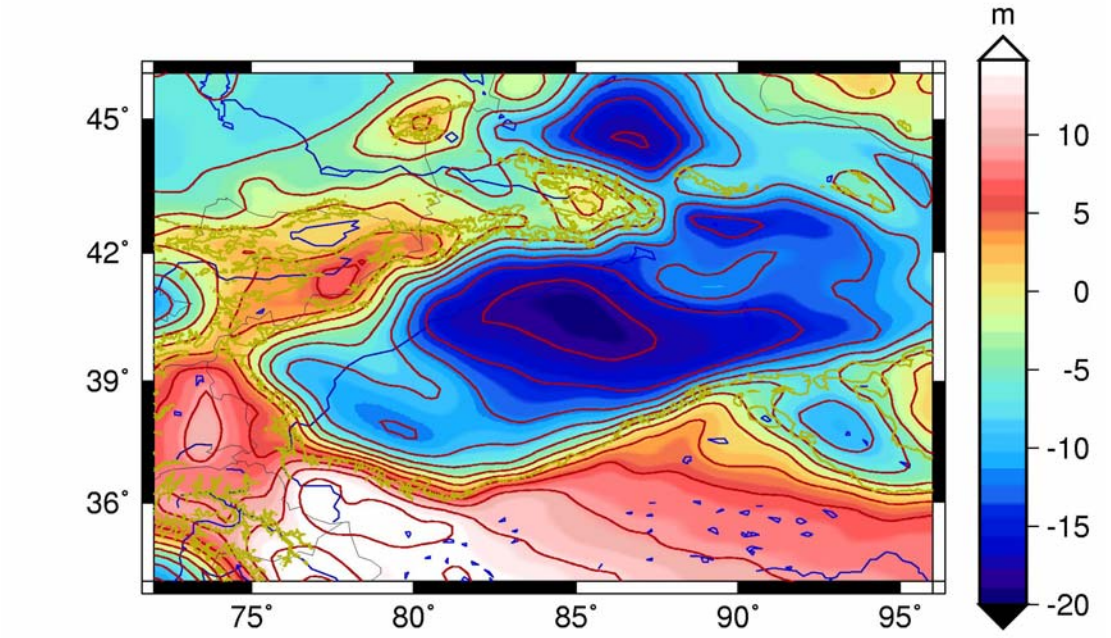

Figure 7.3.4 *Geoid residual (m) for the Tarim basin. Data: EIGEN-GL04C (Förste et al., 2006) freed from lowest degree and order (up to degree and order 10) harmonic components.*

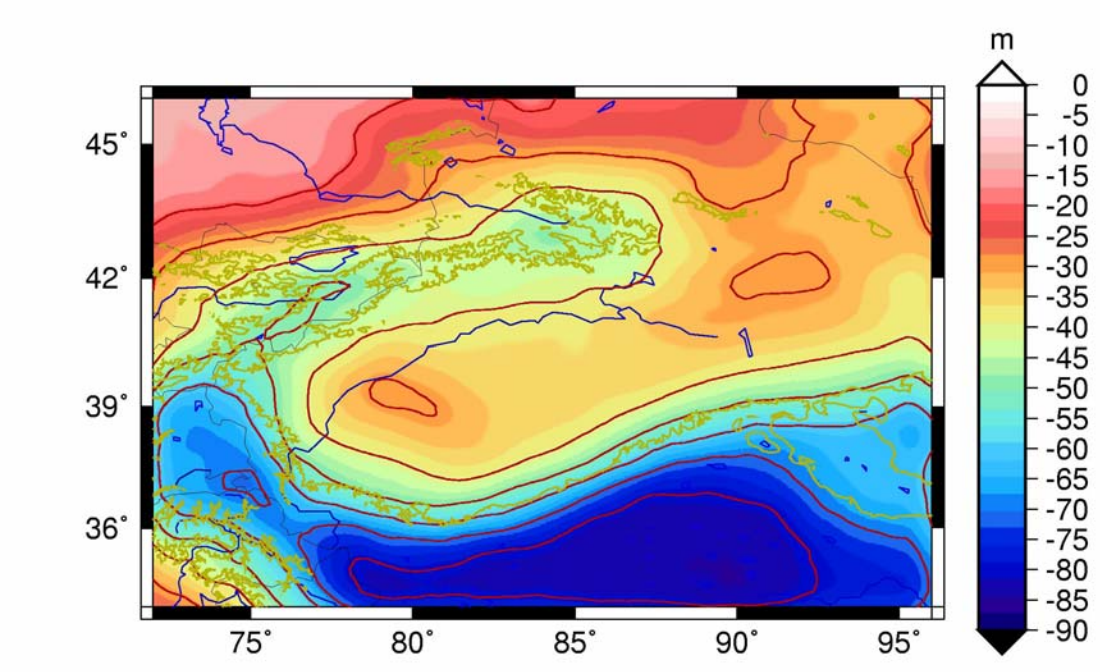

Figure 7.3.5 *Terrain corrected Geoid residual (m) for the Tarim basin. Data: EIGEN-GL04C (Förste et al., 2006) freed from lowest degree and order (up to degree and order 10) harmonic components.*

7.4 Congo basin

The Congo basin, also termed Cuvette centrale, Zaire (Daly et al., 1991;1992) (Fig. 7.4.1a,b) is situated within the Congo craton in Africa and is separated from the Atlantic margin by a 300-km-wide ridge of Precambrian rock. Other cratonic basins on the African continent are the Taoudeni, Chad and Iulmedden basins; the positions of the centres of the interior cratonic basins of Africa are located along a line roughly paralleling but many hundreds of kilometres in-board from the Atlantic margin. The Congo basin is nearly circular in shape with a diameter of about 1500 km, resulting in an area of about 1.8×10^6 km^2. The basin itself is filled with up to 9 km of infra-Cambrian to recent sediments. Whereas the pre-Mesozoic history of the area has been explained tentatively as due to late Proterozoic rifting followed by Paleozoic thermal subsidence (Daly et al., 1992), the Mesozoic-Tertiary history of the basin remains unexplained. The subsidence history is poorly constrained but appears to be rather uniform after an initial period of relatively rapid subsidence in the Late Jurassic (Hartley and Allen, 1994). The 1-km-thick Mesozoic-Cenozoic basin-fill cannot be related genetically to any earlier rift events.

7.4.1 Gravity and geoid of the Congo basin

The Congo basin is a large-scale cratonic basin showing a very evident, nearly circular gravity (Fig. 7.4.2, 7.2.3) and geoid low (Fig. 7.4.4, 7.4.5). A regional study of the gravity field over Africa (Hartley et al., 1996) showed that the Congo basin corresponds also to a pronounced isostatic gravity anomaly that persists also at wavelengths greater than 750 km. The large wavelengths point to a mantle source being partly responsible for the anomaly, as the lithosphere at very long wavelengths responds to loads approximating the local isostatic model. The lithosphere of the Congo Craton is estimated to have a lithospheric effective elastic thickness of about 100 km. Hartley and Allen (1994) propose the term *cold-spot* in order to point to a possible downwelling in the mantle causing the negative isostatic anomaly and a dynamic force to pull down the relatively lighter basin.

The pronounced gravity low and geoid low are in common with the Tarim basin. To have a better picture of the situation, the fields should be corrected for the low-density sedimentary rocks, but detailed information about the sediment thickness is at the moment unavailable for the Congo basin. For this reason any comparison to the West Siberian basin and the Eastern Barents Sea basin can be only tentative and we concentrate in the reminder of comparison between and conclusions from the well-studied areas.

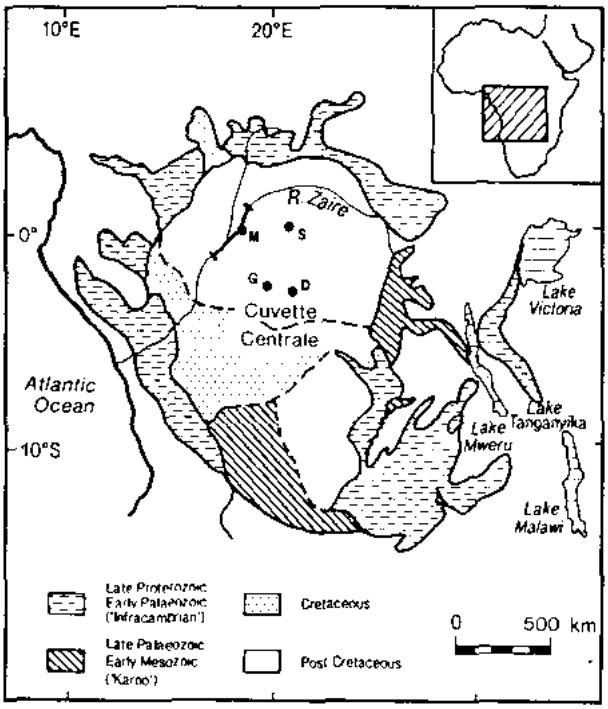

Figure 7.4.1a *Sketch map showing regional geology and location of the Congo Craton (Cuvette Centrale, Zaire) (from Daly al., 1992).*

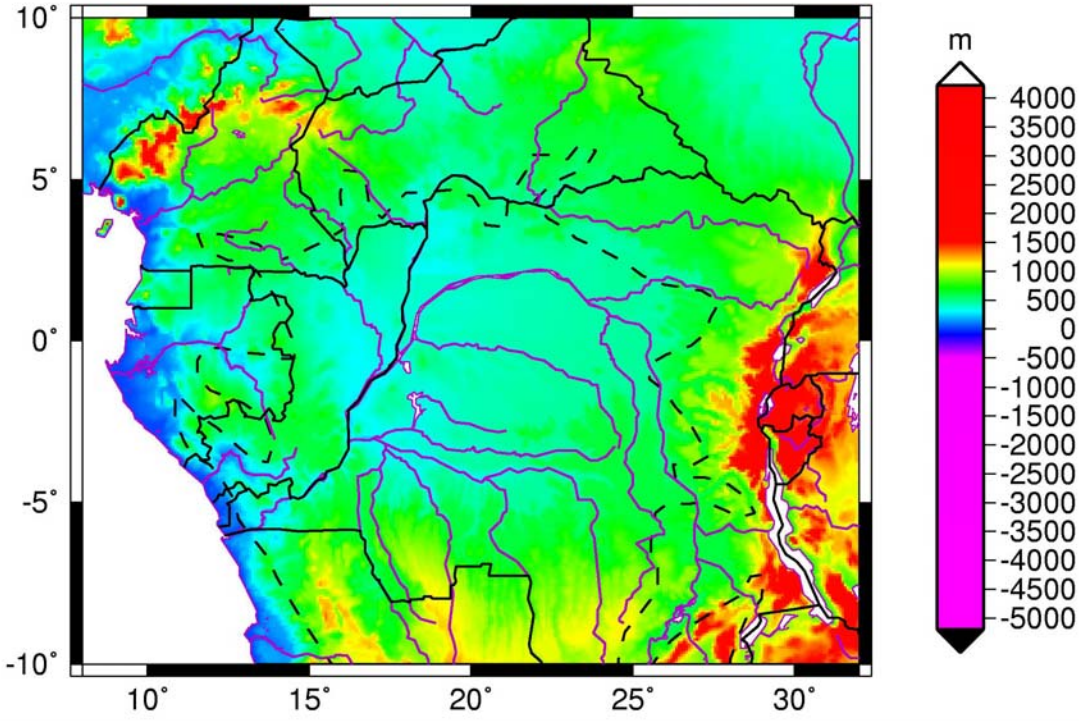

Figure 7.4.1b *Topography of the Congo basin (Cuvette Centrale, Zaire) (basin outline after Daly al., 1992).*

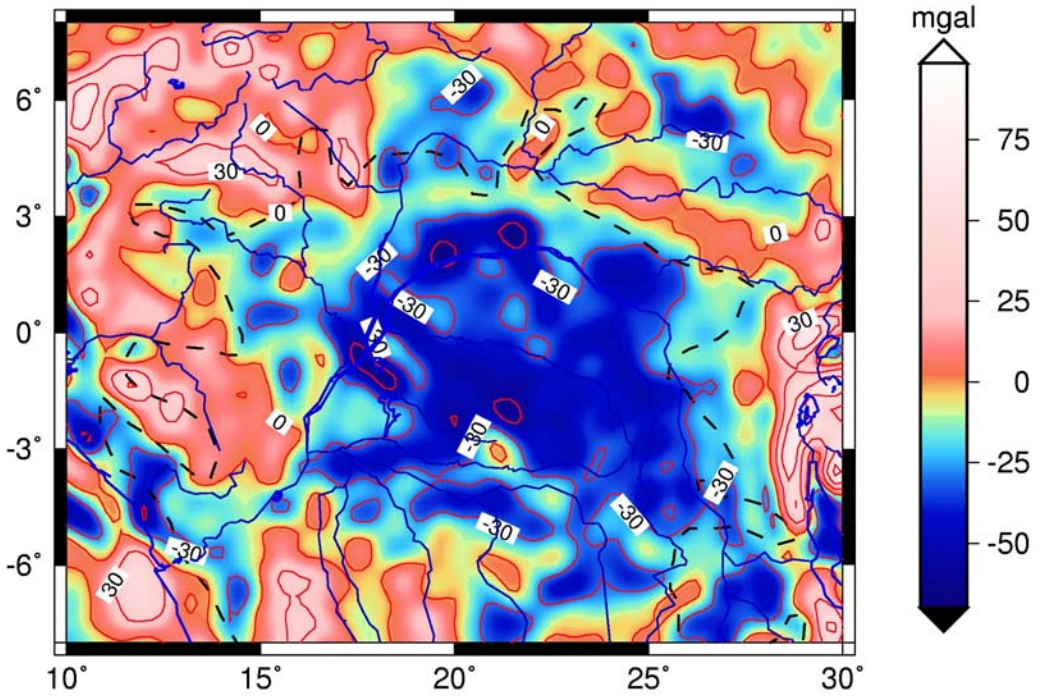

Figure 7.4.2 *Gravity anomaly for the Congo basin (data: EIGEN-GL04C, Förste et al., 2006). Coastline and major rivers in blue.*

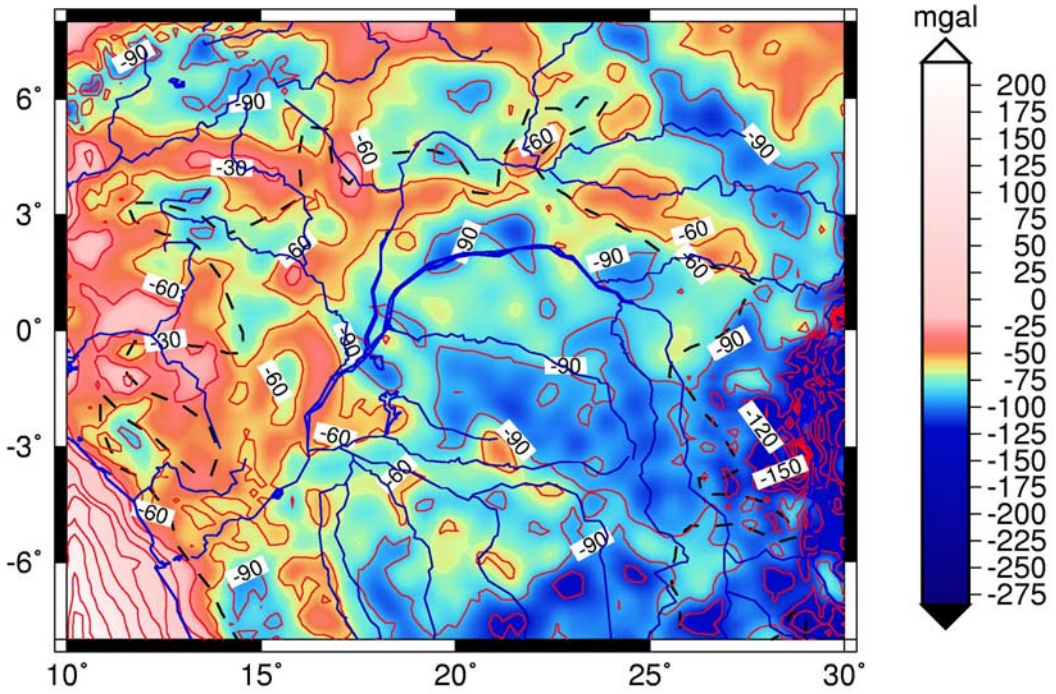

Figure 7.4.3 *Bouguer anomaly (mGal) for the Congo basin. Data: EIGEN-GL04C (Förste et al., 2006).*

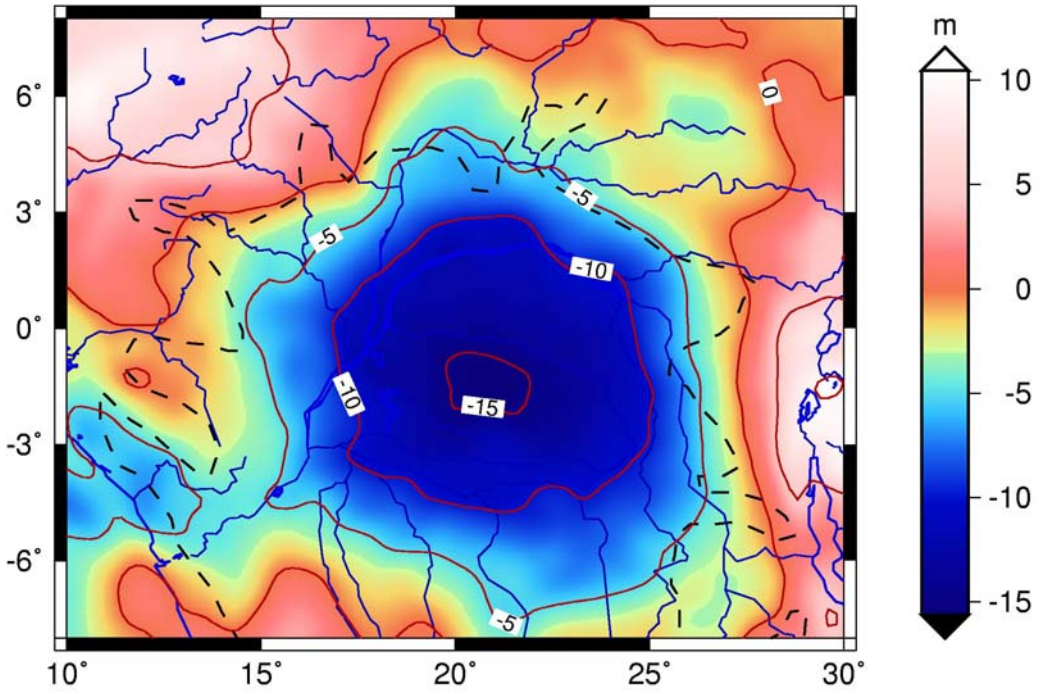

Figure 7.4.4 *Geoid residual (m) for the Congo basin. Data: EIGEN-GL04C (Förste et al., 2006) freed from lowest degree and order (up to degree and order 10) harmonic components.*

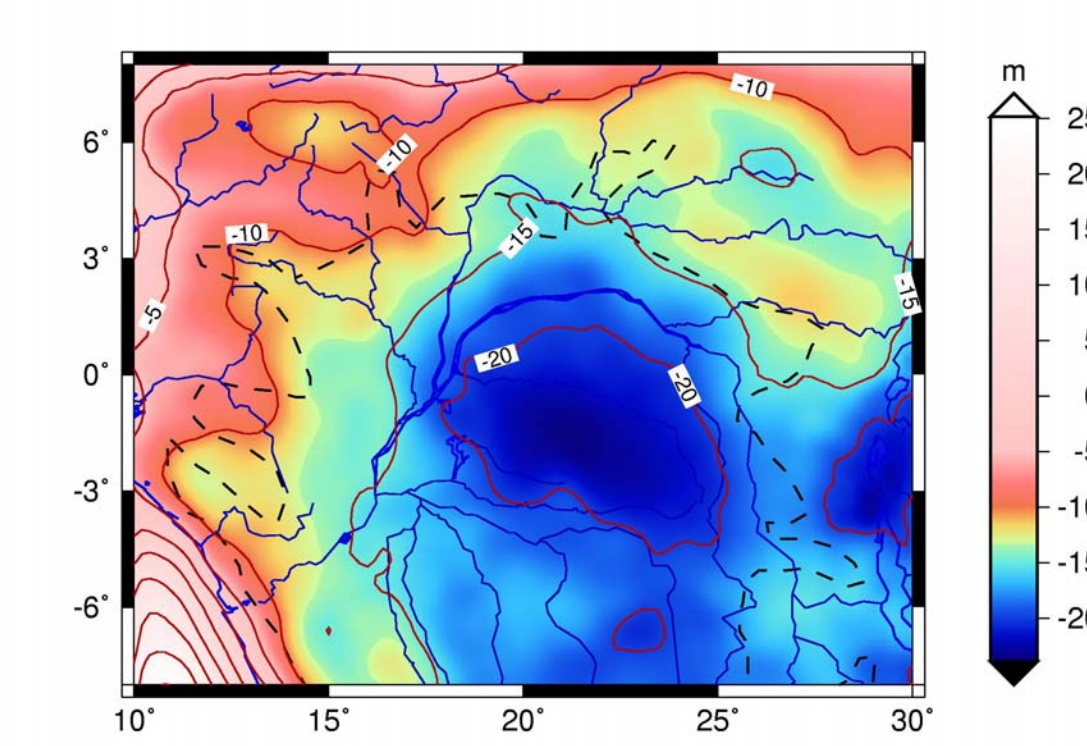

Figure 7.4.5 *Terrain corrected Geoid residual (m) for the Congo basin. Data: EIGEN-GL04C (Förste et al., 2006) freed from lowest degree and order (up to degree and order 10) harmonic components.*

8 CONCLUSIONS

8.1 General Aspects

In this work we have analysed nine large scale sedimentary basins, which are the West Siberian Basin, Tarim, Congo (also termed Zaire), Michigan, Illinois, Amazon, Solimões, Parnaiba and Paranà basins. The basins were studied with respect to areal extension and depth, sedimentary age, presence and age of volcanism, position of volcanic strata with respect to the sedimentary package. Then the gravity field was calculated, comprising the gravity anomaly, Bouguer gravity, the regional and local geoid and the terrain corrected geoid. With the gravity and geoid at hand, a discussion of the isostatic state is made. The detailed study on the West Siberian basin will be the object of the second stage of the present research.

The basin which has been studied very thoroughly in the past is the Michigan basin: ample literature can be found on different theories explaining its subsidence history, and the structure is known from seismic investigations (Zhu and Brown, 1986) and a deep borehole (Sleep and Sloss, 1978). The Michigan basin is one of the smaller basins in aerial extent and thickness of the sediment package, but nonetheless it presents the features found in other large-scale basins, which are: a subsidence history of over 250 Ma, the presence of a volcanic mass along the vertical axis of the sediments, near to concentric elliptical depth isolines of the sediments, a piecewise linear subsidence which alternates continuous subsidence with subsidence stages. The sedimentary layers are flat-lying and undisturbed. The gravity field has a characteristic signature of a general gravity low correlated to the extent to the basin area, with a gravity high crossing or centred in the basin. The Moho is relatively flat and does not respond isostatically to the mass deficit of the sedimentary package.

8.2 Characteristic features of the large scale basins analysed

A list of features found for the Michigan basin is repeatedly found also in the other basins and can be termed typical for large-scale basins. An important point for the sediments evolution is the presence of the volcanism and the relative age of the volcanic strata with respect to the sedimentary package. In all the basins considered, except the Congo basin, volcanic masses are present at some stage and at some depth localised at the basin. Recurrently, the presence of volcanism has been included in the theories aiming at explaining the subsidence and is certainly an important factor for the evolution of large-scale basins. From the analysis of the

South-American basins it is evident that the depth of the volcanic layer is crucial for the productiveness of the basin: the thermal effect of the thick basalt layer (1.5 km) overlying most of the Paranà sediments has rendered the Paranà basin unproductive (Leighton and , 1990) – the Amazon basin, which is of similar age, has the volcanic material at a much shallower depth (Nunn and Aires, 1988) and is productive. Modelling of the thermal evolution of large-scale basin must therefore include the thermal effect of the volcanic material.

The deviation from the classic isostatic equilibrium model that predicts the crustal thickness from the topographic and sedimentary load is a typical feature of the large-scale basins. Detailed models have been formulated for the Paranà, Michigan, Amazon and Congo basins, arriving at the common conclusion that inferred dense material in the lower crust or upper mantle contributes to the isostatic equilibrium, the crustal thickness remaining rather flat and with greater thickness (greater than 40 km) than he normal reference crust (35 km). High density masses in the crust and mantle are therefore a typical feature. The study of the gravity and geoid fields is thus an essential tool in understanding the structure of this type of basins.

Typical gravity anomaly values for the basins are between -30 and -50 mGal. A subset of basins of our grouping (Amazon, West Siberian Basin, Michigan and Illinois) presents a linear gravity high, which can reach +50 mGal. The attributed explanation to this signal is an extinct rift beneath the basins. The geoid undulations show greater variability, and in several cases are in evident correlation with the basins. Among those studied, definite and pronounced geoid lows are found for the West Siberian, Amazon, Parana', Tarim and Congo basins. In the other cases, the geoid reveals a variation at larger scale, that reveals no evident correlation with the basin, as is the case for the Parnaiba, Michigan and Illinois basins.

8.3 Common features and implications for the East Barents Sea basin

The deviation from isostatic equilibrium, the high-density upper mantle densities, and the relatively flat and deep Moho were results obtained (Ebbing et al., 2005, 2006) by the isostatic and density inversion modelling of the Eastern Barents Sea and by seismologic investigations, respectively. In the case this property were typical of all large scale basins, the analysis of the isostatic state can be used for distinguishing between basins formed in a

extensive stress regime (e.g. rifting) from the basins formed by the interplay of vertical forces due to a combination of heating and loading.

The presence of an underlying extinct rift and significant quantities of volcanic material for the Eastern Barents Sea (Ivanova et al., 2006) allows a comparison to the Michigan basin. The Michigan Basin and the Eastern Barents Sea basin are relatively small with regard to the geographical extension, compared to the other intracratonic basins. Clearly, For both basins the rifting process plays an important role in the early stage and/or initiation of the basin formation. However, the Michigan basin has only a maximum thickness of 3.5 km, while the Eastern Barents Sea basins locally exceed 20 km in depth. Even with the suggested erosion in the Michigan basin (Sloss and Scherer, 1975) the total thickness is not in the same range as for the Eastern Barents Sea. The continuous subsidence in the Michigan basin is explained by free-thermal convection, which initiates pulses of subsidence (Nunn 1994). O'Leary et al. (2004) explain the subsidence histories of the South and North Eastern Barents Sea basins by intermittent phases of lithospheric extension as they share the tectonic histories, at least for pre-Triassic times, and convective drawdown caused by the pulling of lithosphere toward the zone of maximum shortening, should have led to continuous subsidence. However, the present-day picture of the crustal structure of the Eastern Barents Sea basin makes such an interpretation speculative. Similar to the Michigan basin, the lower crust and upper mantle is interpreted to have relatively high densities. This may be associated to intrusions of hot asthenospheric material that may have metamorphosed the lower crust or was emplaced in the lower crust. The magnetic anomaly of the Barents Sea (Fig. 1.2) may point to the presence of intrusions in the basement at the western flank of the Eastern Barents Sea basins. If high-density material was formed or emplaced at the base of the crust the present-day geometry of the Moho may be a response to increased loading by the high-density material. As the system was becoming stable the flexural rigidity increased leading to the platform formation. This may also have caused the observed changes in vertical subsidence between the Eastern and Western Barents Sea.

9 OUTLOOK

The present results of the screening of other large scale basins gives a solid basis on which to rely for the further investigations concerning the West Siberian and the Eastern Barents Sea basins.

The modelling of the gravity field of the West Siberian Basin will give insight into the underlying structure of the basin. The input data will be the combined satellite-terrestrial gravity field and geoid undulation, the 1km-grid digital elevation model, the basement depth model (Statoil compilation), the detailed basement depth recorded in the seismic lines and the Moho depth published by Vyssotski et al. (2006). A density model will be established that includes the sediment package (formulating density depth variation by compaction), the basalt layer, and the crustal thickness variations. For the density modelling we will have a qualitative estimate of the density variations at the lower crust or upper mantle. We will focus on the linear positive gravity anomalies, which can be related to rifts visible in the seismic profiles published by Vyssotski et al. (2006). Considering the Bouguer gravity field, we find an inverse relation between the Bouguer anomalies and the sediment thickness: where the basement is deepest the Bouguer is relatively more positive (northern part of the basin) with respect to the shallower basement (e.g. south-eastern part of the basin). This situation demands lateral variations on the crustal density below the basin and thus is an indication of different terranes underlying the basin. The density model will allow us to fulfil the isostatic calculations and obtain a further differentiation of the terranes composing the West Siberian basin.

For the Barents Sea Region new regional models of the lithospheric structure will be made available from the new PETROBAR project. As a continuation of the ongoing project and the Barents3D compilation (Ritzmann et al. 2006) the new model will provide a basis for studying the lithospheric structure in more detail. Detailed regional key transects which combine the basin configuration with the deep crustal and upper mantle structure will allow reconstructing the basin formation history of the Eastern Barents Sea basin. Hereby, the inherited mantle structure is a key to unveil the post-rift evolution and subsidence history of the Eastern Barents Sea basin in detail. Especially, changes in the flexural rigidity with time due to thermal and tectonic events have to be considered to construct the present-day crustal configuration and potential field signal.

ACKNOWLEDGEMENTS

Laura Marello and Federica Fratepietro are thanked for the preparation of figures and graphs. Ildiko' Nagy is thanked for assistance in the bibliographic search and retrieval of documents. Hans Morten Bjørnseth and Christine Fichler from Statoil initiated our study and supplied us with information on the studied areas. We appreciate the assistance and help from all these persons and especially Statoil for funding the study. We acknowledge the use of the GMT-mapping software of Wessel and Smith (1998).

REFERENCES

Ahern J.L. & Dikeou P.J. 1989: Evolution of the lithosphere beneath the Michigan Basin, Earth and Planetary Science Letters, 95, 73-84.

Allen, P.A., & Allen, J.R. 2005: Basin analysis: Principles and Applications, 2nd edition. Blackwell Publishing, Oxford, 549p.

Almeida, F.F.M., Hasui, Y., De Brito Neves, B.B. & Fuck R.A. 1981: Brazilian structural provinces : An introduction. Earth Science Reviews, 17, 1-29.

Almeida, F.F.M., De Brito Neves, B.B. & Dal Rè Carneiro, C. 2000: The origin and evolution of the South American Platform. Earth Science Reviews, 50, 77-111.

An, M. & Assumpção, M. 2006: Crustal and upper mantle structure in the intracratonic Parana' basin, SE Brazil, from surface wave dispersion using genetic algorithms. J. S. Am. Earth Sc., 21, 173-184.

Assumpção, M., James, D.E. & Snoke, J.A. 2002: Crustal thickness in SE Brazilian shield by receiver function analysis: implications for isostatic compensation. J. Geophys. Res. 107 (B1), 2006. 10.1029/2001JB000422.

Bassin, C., Laske, G. & Masters, G. 2000: The Current Limits of Resolution for Surface Wave Tomography in North America, EOS Trans AGU, 81, F897.

Baturin, D., Vinogradov, A. & Yunov, A. 1991: Tectonics and hydrocarbon potential of the Barents Megatrough. *American Association of Petroleum Geologists Bulletin* **75**, 1404.

Bedle, H. & van der Lee, S. 2006: Fossil flat-subduction beneath the Illinois basin, USA. Tectonophysics, 424, 53-68.

Braitenberg, C., Wang, Y., Fang, J., & Hsu, H.T. 2003: Spatial Variations of flexure parameters over the Tibet-Quinghai Plateau. Earth Planet. Sci. Lett., 205, 211-224.

Chen, Z.Q. & Shi, G.R. 2003: Late Paleozoic depositional history of the Tarim basin, northwest China: an integration of biostratigraphic and lithostratigraphic constraints. AAPG Bulletin, 87, 1323-1354.

Cordani, U.G., Brito Neves, B.B., Fuck, R.A., Porto, R., Filho, A.T. & Cunha, F.M.B. 1984. Estudo preliminar de integracção do pre´-Cambriano com os eventos tectonicos das bacias sedimentares brasileiras. Rev. Ciencia Tecnica Petroleo, 15. Petrobras, CENPES, Rio de Janeiro.

Crust 2.0 2006: http://mahi.ucsd.edu/Gabi/rem.html

Daly M.C., Lawrence, S.R. Kimuna, D. & Binga M. 1991: Late Paleozoic deformation in central Africa: a result of a distant collision? Nature, 350, 605.

Daly M.C., Lawrence, S.R., Diemu-Tshiband, K.& B. Matouana 1992: Tectonic evolution of the Cuvette Centrale, Zaire. J. Geol. Soc. London, 149, 539-546.

Ebbing, J., Braitenberg, C. & Skilbrei, J.R. 2005: Basement characterisation by regional isostatic methods in the Barents Sea. NGU Report 2005.074, p.78

Ebbing, J., Braitenberg, C., Bjørnseth H.M., Fichler, C. & Skilbrei J.R. 2006: Basement Characterisation by Regional Isostatic Methods in the Barents Sea. EAGE/EAGO/SEG Conference, Saint Petersburg.

Ebbing, J., Braitenberg, C., Wienecke, S., in prep: Insights into the lithospheric structure and the tectonic setting of the Barents Sea region by isostatic considerations. In prep. for GJI.

Feng, M., Assumpção, M., & Van Der Lee, S. 2004: Group-velocity tomography and lithospheric s-velocity structure of the south american continent. Phys. Earth Planet. Int. 147 (4), 315–331. doi:10.1016/j.pepi.2004.07.008.

Forsberg, R. 1984: A Study of Terrain Reductions, Density Anomalies and Geophysical Inversion Methods in Gravity Field Modelling. Reports of the Department of Geodetic Science and Surveying, No. 355, The Ohio State University, Columbus, Ohio, 1984.

Förste, C., Flechtner, F., Schmidt, R., König, R., Meyer, U., Stubenvoll, R., Rothacher, M., Barthelmes, F., Neumayer, H., Biancale, R.. Bruinsma, S., Lemoine, J.-M. & Loyer, S. 2006: A mean global gravity field model from thecombination of satellite mission and altimetry/gravimetry surface data – Eigen-GL04C. Geophysical Research Abstracts, Vol. 8, 03462, 2006

Guo, Z.-J., Yin, A., Robinson, A., Jia, C.-Z. 2005: Geochronology and geochemistry of deep-drill-core samples from the basement of the central Tarim basin. J. of Asian Earth Sci.. 25, 45–56.

Hartley, R.W. & Allen, P.A. 1994: Interior cratonic basins of Africa: relation to continental break-up and role of mantle convection. Basin Res., 6, 95-113.

Hartley, R.W., Watts, A.B. & Fairhead, J.D. 1996: Isostasy of Africa. Earth Planet. Sci. Let., 137, 1-18.

Haxby, W.F., Turcotte, D.L. & Bird, J.M. 1976: Thermal and mechanical evolution of the Michigan Basin. Tectonophysics, 36, 57-75.

Ivanova, N.M., Sakoulina, T.S. & Roslov, Yu.V. 2006:. Deep seismic investigation across the Barents–Kara region and Novozemelskiy Fold Belt (Arctic Shelf). *Tectonophysics,* 420, 123–140.

Jia D., Lu H., Cai D., Wu S., Shi Y. & Chen C. 1998: Structural features of northern Tarim basin: Implications for regional tectonics and petroleum traps. AAPG Bulletin, 82, 1, 147-159.

Johansen, S.E., Ostisty, B.K., Birkeland, Ø., Fedorovsky, Y.F., Martirosjan, V.N., Christensen, O. B., Cheredeev, S.I., Ignatenko, E.A. & Margulis, L.S. 1992: Hydrocarbon potential in the Barents Sea region: play distribution and potential. In: Arctic Geology and Petroleum Potential (Vorren, T.O., Bergsager, E., Dahl-Stamnes, Ø.A., Holter, E., Johansen, B., Lie, E. and Lund, T.B. eds.). *NPF Special Publication 2,* 273-320. Elsevier, Amsterdam.

Kovylin, V.M. 1985: Fault-block structure of the West Siberian Craton and its petroleum potential. Sovetskaya geologiya 2, 77–86. [in Russian].

Leighton M.W. & Kolata D.R. 1990: Selected interior cratonic basins and their place in the scheme of global tectonics, Mem. Am. Ass. Petrol Geol., 51, 729-797.

Lithospheric Dynamic Atlas of China 1989: China Cartographic Publishing House, Beijing.

McKenzie, D. 1978: Some remarks on the development of sedimentary basins. *Earth and Planetary Science Letters*, 40, 25-32.

Milani, E.J. & Thomaz Filho, A. 2000: Sedimentary basins of South America. In: Cordani U.G., Milani E.J., Thomaz Filho, A. & Campos D.A.: Tectonic evolution of South America, p.389-449, Rio de Janeiro, 2000.

Milani, E.J. & Ramos, V.A. 1998: Orogenias paleozòicas no domìnio sul – ocidental do Gondwana e os ciclos de subsidència da Bacia do Paranà. Revista Brasileira de Geociències, 474-484.

Nunn, J.A. 1994: Free thermal convection beneath intracratonic basins: thermal and subsidence effects. Basin Research, 6, 115-130.

Nunn, J.A. & Aires, J.R. 1988: Gravity anomalies and flexure of the lithosphere at the middle Amazon basin, Brazil. J. Geophys. Res., 93, 415-428.

Nunn, J.A. & Sleep, N.H. 1984: Thermal contraction and flexure of intracratonal basins: a three-dimensional study of the Michigan basin. Geophys. J. R. Astr. Soc., 76, 587-635.

O'Leary, N., White, N., Tull, S. & Bashilov, V. 2004: Evolution of the Timan–Pechora and South Barents Sea basins. *Geol. Mag.*, 141 (2), 141–160.

Ostisty, B. K. & Cheredeev, S. I. 1993: Main factors controlling regional oil and gas potential in the west Arctic, former USSR. In *Basin modelling: advances and applications* (eds A. G. Dore *et al.*), pp. 591– 7. Norwegian Petroleum Society, Special Publication No. 3.

Otto, S. C. & Bailey, R. J. 1995: Tectonic evolution of the northern Ural Orogen. *Journal of the Geological Society, London* 152, 903–6.

Reichow, M.K., Saunders, A.D., White, R.V., Al'Mukhamedov, A.I. & Medvedev, A.Y. 2005: Geochemistry and petrogenesis of basalts from the West Siberian Basin: an extension of the Permo–Triassic Siberian Traps, Russia . *Lithos*, 79, 425-452.

Ritzmann, O., Maecklin, N., Faleide, J.I., Bungum, Mooney, W.D. & Detweiler, S.T. 2006: A 3D geophysical model for the crust in the greater Barents Sea region: Database compilation, model construction and basement characterization. Submitted to GJ

Sleep N.H. & Sloss, L.L. 1978: A deep borehole in the Michigan Basin. J. Geophys. Res., 83, B12, 5815-5819.

Sleep N.H. & Snell, N.S. 1976: Thermal contraction and flexure of mid-continent and Atlantic marginal basins. Geophys. J. R. Astr. Soc., 45, 125-154.

Sleep, N.-H, Nunn J.-A., Chou-Lei 1980: Platform basins. Annual Review of Earth and Planetary Sciences. 8; Pages 17-34.

Sloss L.L. & W. Scherer 1975: Geometry of sedimentary basins: applications to the Devonian of North America and Europe, Geol. Soc. Am., Memoir, 142, 71-88.

Sobel E.R., Hilley, G.E. & Strecker, M.R. 2003: Formation of internally drained contractional basins by aridity-limited bedrock incision. J. Geophys. Res., 108, B7, 2344, doi:10.1029/2002JB001883,

Tscherning, C.C., Forsberg, R. & Knudsen, P. 1992: The GRAVSOFT package for geoid determination. Proc. 1. Continental Workshop on the Geoid in Europe, Prague, May 1992, pp. 327-334, Prague.

Turcotte D.L. & Angevine C.L. 1982: Thermal mechanism of basin formation. Phil. Trans. R. Soc. Lond. A 305, 283-294.

Verhoef, J., Roest, W.R., Macnab, R., Arkani-Hamed, J. & Members of the Project Team 1996: Magnetic anomalies of the Arctic and North Atlantic Oceans and adjacent land areas. *GSC Open File 3125, Parts a and b* (CD-ROM and project report), Geological Survey of Canada, Dartmouth NS.

Vyssotski A.V., Vyssotski, V.N. & Nezhdanov, A.A. 2006: Evolution of the West Siberian Basin. Marine and Petroleum Geol., 23, 93-126.

Watts A.B., Karner G.D. & Steckler M.S. 1982: Lithospheric flexure and evolution of sedimentary basins. Phil. Trans. R. Soc. Lond. A 305, 249-281.

Watts, A.B. 2001: Isostasy and flexure of the lithosphere, Cambridge University Press, Cambridge, 2001, 458 pp.

Wessel, P., & Smith, W. H. F. 1998: New, improved version of Generic Mapping Tools Released. EOS Trans., AGU, 79 (47), p. 579.

Yuzhu K. & Zhihong K. 1996: Tectonic evolution and oil and gas of Tarim basin. Journal of Southeast Asian Earth Sciences, 13, 3-5, 317-325.

Zhu T. & L.R. Brown 1986: Consortium for continental reflection profiling Michigan Surveys: reprocessing and results. J. Geophys. Res., 91, 11477-11495.